Journal of Controlled Release 337 (2021) 431–447

Contents lists available at ScienceDirect

Journal of Controlled Release

journal homepage: www.elsevier.com/locate/jconrel

Polyethylene glycol-based linkers as hydrophilicity reservoir for antibody-drug conjugates

T. Tedeschini [a], B. Campara [a], A. Grigoletto [a], M. Bellini [a], M. Salvalaio [a], Y. Matsuno [b], A. Suzuki [b], H. Yoshioka [b], G. Pasut [a,*]

[a] University of Padova, Dept. Pharmaceutical Sciences, Via Marzolo 5, 35131 Padova, Italy
[b] NOF CORPORATION, DDS Research Laboratory, 3-3 Chidori-Cho, Kawasaki-Ku, Kawasaki, Kanagawa 210-0865, Japan.

ARTICLE INFO

Keywords:
Antibody-drug conjugates
Drug-linker design
PEGylation
Stability study
Pharmacokinetics

ABSTRACT

Antibody-drug conjugates (ADCs) are an established therapeutic entity in which potent cytotoxic drugs are conjugated to a monoclonal antibody. In parallel with the great emphasis put on novel site-specific bioconjugation technologies, future advancements in this field also rely on exploring novel linker-drug architectures that improve the efficacy and stability of ADCs. In this context, the use of hydrophilic linkers represents a valid strategy to mask or reduce the inherent hydrophobicity of the most used cytotoxic drugs and positively impact the physical stability and *in vivo* performance of ADCs. Here, we describe the use of linkers containing monodisperse poly(ethylene glycol) (PEG) moieties for the construction of highly-loaded lysine-conjugated ADCs. The studied ADCs differ in the positioning of PEG (linear or pendant), the bonding type with the antibody (amide or carbamate), and the drug-to-antibody ratio (DAR). These ADCs were first evaluated for their stability in solution under thermal stress, showing that both the drug-linker-polymer design and the nature of the antibody-linker bonding are of great importance for their physical and chemical stability. Amide-coupled ADCs bearing two pendant 12-unit poly(ethylene glycol) chains within the drug-linker structure were the best performing conjugates, distancing themselves from the ADCs obtained with a conventional linear 24-unit PEG oligomer or the linker of Kadcyla®. The pharmacokinetic profiles of amide-linked ADCs, with a linear or pendant configuration of the PEG, were tested in mice in comparison to Kadcyla®. Total antibody pharmacokinetics paralleled the trends in aggregation tendency, with slower clearance rates for the ADCs based on the pendant drug-linker format. The above-mentioned findings have provided important clues on the drug-linker design and revealed that the positioning and configuration of a PEG unit have to be carefully tuned to achieve ADCs with improved stability and pharmacokinetics.

1. Introduction

Antibody-drug conjugates (ADCs) represent an emerging therapeutic approach in cancer treatment that combines the specificity of monoclonal antibodies (mAbs) with the intrinsic killing properties of potent cytotoxic drugs [1–3]. Since the first studies with relatively common cytotoxic drugs, such as methotrexate and doxorubicin, linked to polyclonal antibodies, adequate improvements have progressively been made to face some limitations and imperfections of the first generations of ADCs. After the groundbreaking impact of the two FDA- and EMA-approved ADCs, Seattle Genetics' brentuximab vedotin (Adcetris®) in 2011 [4] and Genentech's ado-trastuzumab emtansine (Kadcyla®) in 2013 [5], the field has been expanding, leading now to more than 100 candidates in clinical trials and the approval of a total of 5 ADCs and to the preregistration of other 6 by FDA [6–11].

Besides the selection of appropriate targets [12] and optimal antibody characteristics [2], the success of an ADC is dictated by other key features such as the linker chemistry [13–17], the site of attachment on the antibody [18], and drug-to-antibody ratio (DAR) [19,20]. Drug loading is well-known to be a critical parameter of any ADC as the lipophilic nature of the most used cytotoxic agents poses a threat to the biophysical and pharmacological properties of the entire ADC molecule. The conjugation of these hydrophobic entities to antibodies may, in effect, lead to physical instability (*i.e.* aggregation) [21–23] and, ultimately, compromise the ADC *in vivo* performance [19,20,24,25]. The linker itself might also bring additional hydrophobicity to the construct,

* Corresponding author.
E-mail address: gianfranco.pasut@unipd.it (G. Pasut).

https://doi.org/10.1016/j.jconrel.2021.07.041
Received 28 June 2021; Received in revised form 21 July 2021; Accepted 23 July 2021
Available online 27 July 2021

outlining an even worse scenario [26]. As a consequence, the average DAR has long been limited to the range of 2–4 drug molecules per antibody, considered to be the optimal trade-off for achieving maximum therapeutic index and, at the same time, a good ADC stability [19].

While cytotoxic agents rely on their hydrophobic modules to retain their interactions and consequent activity, there is much leeway to engineer the linker moiety to tackle the overall hydrophobicity of the drug-linker and overcome the limiting tie of a restrained drug loading [27]. Innovative hydrophilicity sources have been explored in various linker frameworks and with different warheads, resulting in ameliorated physicochemical properties [28], favorable PK profiles [25,29,30], major tolerability [31], evasion of MDR1-related resistance [26,32], and efficacy in heterogeneous tumors [33,34]. Current approaches mainly involve the inclusion of hydrophilic discrete polymeric groups, such as polyethylene glycol (PEG), at different lengths and/or configurations in the linker scaffold, although examples of highly complex polymeric platforms have also been reported recently [35].

Given the great success of PEGylation within protein therapeutics [51,36–38], the incorporation of PEG into the linker structure of ADCs appears to be the most attractive strategy for masking the intrinsic hydrophobicity of the most used payloads (maytansinoids, auristatins, *etc.*). It is worth noting, though, that the PEG segment in the linker scaffold needs to fulfill precise requirements to be effective. Within this context, the PEG configuration, length and positioning in the linker have demonstrated to be of great importance, and so has their synergistic effect [25,29]. Particularly, an extended PEG spacer placed between the antibody and the drug seems to be inadequate as a hydrophobicity balancing element [25]. More recently, a detrimental effect of a linear orientation was also observed for a twelve-unit monodisperse polysarcosine ($PSAR_{12}$)-based linker [39]. Still, smaller PEG spacers ($\leq PEG_7$) have worked flawlessly in some examples [31,33]. These results together suggest that there is a tight correlation between the polymer length and its placement in the linker structure. A PEG chain in a loose and flexible design would better shield the payload's hydrophobicity as opposed to being a long, fixed stretcher that distances the drug from the antibody.

In the present work, we propose a novel monodisperse PEG linker system in which the polymer is shaped as two PEG_{12}-capped pendant side chains within the drug-linker framework, midway the antibody and the cytotoxic agent. We envisioned that this innovative pendant PEG conformation could guarantee the optimal shield against the hydrophobic burden derived by the conjugation and allow for the preparation of highly loaded ADCs with decreased aggregation tendency and untouched pharmacokinetic profile. Given the high and variable

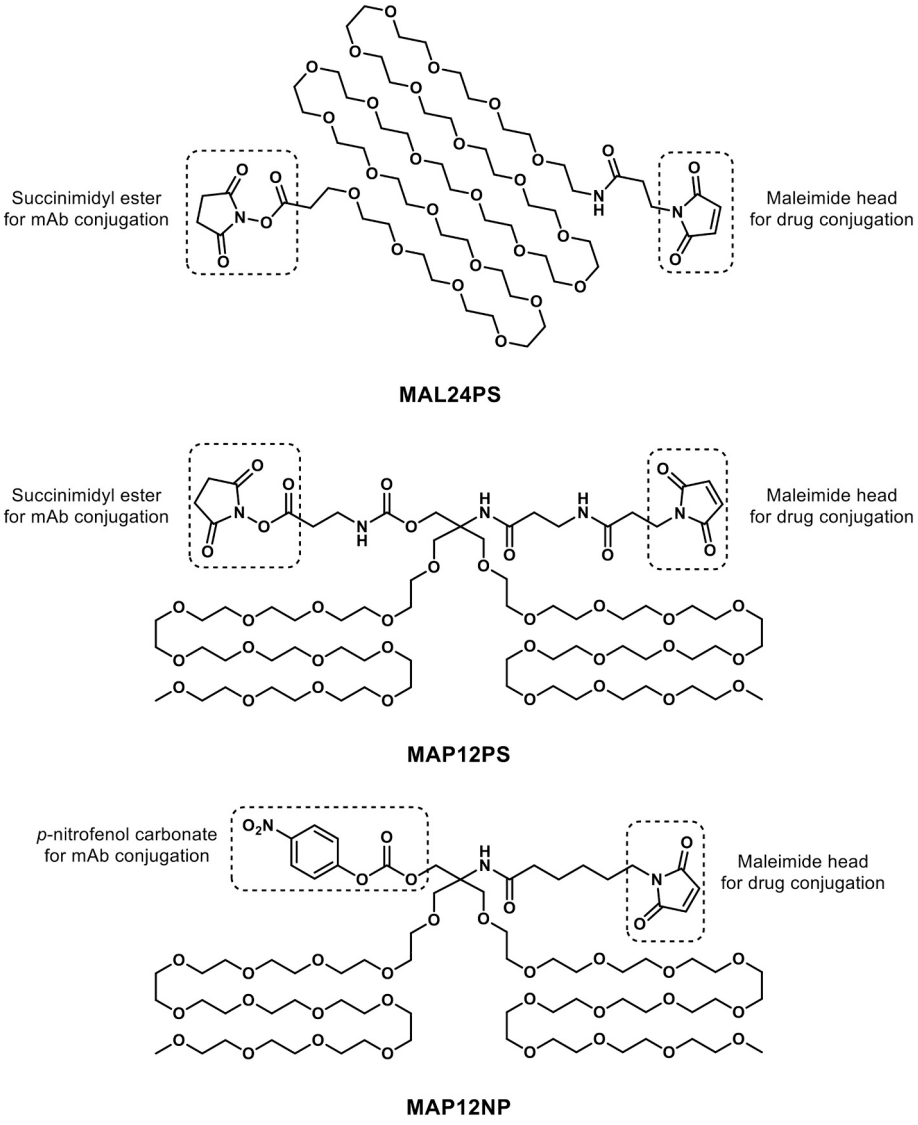

Fig. 1. Structures of the PEG-linkers: the linear PEG linker MAL24PS and the pendant PEG linkers MAP12PS and MAP12NP. Reactive functional groups are circled with dashed lines.

hydrophobicity penalty that a profuse lysine-based conjugation may lead to [20], we believed that a lysine-linked ADC would offer the optimal model to test this innovative linker platform. Moreover, to the best of our knowledge, the configuration-dependent effects of PEG on lysine-conjugates have not been explored yet. In the first design, a classic maleimide ring and an N-hydroxysuccinimide (NHS)-activated ester group were included as orthogonal conjugation handles for drug and antibody, respectively. In a second design, a *p*-nitrophenol (*p*NP)-activated carbonate group was used in place of the succinimidyl ester to probe the stability of the resultant carbamate linkage with antibody lysine residues compared to the traditional amide coupling. In this pilot study, we used mertansine (DM1) as an exemplary hydrophobic drug and the anti-HER2 mAb Trastuzumab (Trs) as an exemplary antibody and constructed lysine-conjugated ADCs using either the new PEG_{12} pendant linker in its two variants (MAP12PS or MAP12NP, Fig. 1) or a conventional discrete PEG_{24} linear linker (MAL24PS, Fig. 1). We prepared both the low DAR (3–4) version and the high-DAR (7–8) version of the PEGylated conjugates to see the impact of PEG orientation at different drug loadings on physical stability and *in vivo* pharmacokinetics and compared the same to the marketed lysine-conjugate Kadcyla® and two in-house Kadcyla® analogs prepared in our laboratories. In this study, we provide a thorough analysis of the physical stability, *i.e.*, aggregation, of lysine-conjugated ADCs bearing different linkers and having different DARs. We also show evidence of a direct relationship between the physical stability and the *in vivo* pharmacokinetic profile of a conjugate, illustrating that less stable ADCs possess faster plasma clearance. Lastly, we present data on the concrete benefit of using a PEG molecule shaped as two pendant side chains within the linker structure to reach high DAR values while preserving stability and antibody pharmacokinetics.

2. Materials and methods

2.1. Materials

Commercially available Herceptin® (Trastuzumab; Genentech) and Kadcyla® (ado-trastuzumab emtansine, T-DM1; Genentech) were purchased from a pharmacy. Upon arrival, both Herceptin® and Kadcyla® were reconstituted with water for injection USP at a concentration of 21 mg/mL and 20 mg/mL, respectively. They were aliquoted, snap-frozen and stored at −80 °C until further use.

PEG linkers (PUREBRIGHT® MA-P12-PS, MA-P12-NP and MA-L24-PS) were manufactured and supplied by NOF CORPORATION (Tokyo, Japan). 50 mg/mL solutions of MAP12PS, MAP12NP and MAL24PS in DMSO were stored in tightly sealed conditions (−20 °C, with N_2 protecting the atmosphere inside the vials) before use. DM1 (N_2'-deacetyl-N_2'-(3-mercapto-1-oxopropyl)-maytansine), was purchased from MedChemExpress (New Jersey, USA); accurately weighed amounts of DM1 were dissolved in DMA (*N*,*N*-dimethylacetamide) to prepare 50 mg/mL DM1 stock solutions. SMCC (succinimidyl 4-(*N*-maleimidomethyl) cyclohexane-1-carboxylate) was purchased by Thermo Fisher Scientific (Waltham, MA, USA). 50 mg/mL stock solutions of SMCC in DMSO were stored in tightly sealed conditions (−20 °C, with N_2 protecting atmosphere).

2.2. Notations

In the ADCs described here, the mAb Trs is connected *via* lysine residues to one end of the bifunctional linker through either an amide or a carbamate bond while the maytansinoid DM1 is connected to the other end of the linker through a thioether bond. The ADCs are assigned the following nomenclature where the mAb, the linker used, and the DAR value are included to identify the conjugate: "T" for Trs, "L_{24}" or "$P_{(12\times2)}$ for the type of PEG linker, and (linker-DM1)n for the average degree of conjugation. The letter "c" in italic preceding the PEG linker type will specify the carbamate-coupled ADCs. In-house ADCs featuring the SMCC linker respect the same notation scheme, except the linker is identified as "MCC". DM1-linker products are identified by the notation "DM1 + complete linker acronym".

2.3. Preparation and preliminary characterization of the ADCs

2.3.1. Two-step conjugation procedure

T-(L_{24}-DM1)$_3$, T-($cP_{(12\times2)}$-DM1)$_3$ and in-house Kadcyla® (T-(MCC-DM1)$_3$) were prepared following Kadcyla®'s conjugation procedure [21]. As an example, here follows the preparation of T-(L_{24}DM1)$_3$. Briefly, Trs (8 mg/mL in 50 mM sodium phosphate, 50 mM NaCl, 2 mM EDTA, pH 6.5, hereafter referred to as "Buffer 1″) was reacted with 10.5-fold molar excess MAL24PS linker with gentle stirring for 4 h at 20 °C. The unreacted linker was removed by using Amicon® 30 kDa Ultra Centrifugal filters. The extent of modification (linker-to-antibody ratio, LAR) was assessed by MALDI-TOF mass analysis and the modified antibody's concentration was assessed through Bicinchoninic acid assay (BCA assay) using Trs as standard. The modified antibody was then reacted with a 1.7-fold excess of DM1 per linker molecule. The reaction was carried out at 10 mg/mL antibody concentration in Buffer 1 (94% *v*/v) with DMA (6% v/v) and incubated with gentle stirring for 17.5 h at 20 °C. The conjugation mixture was gel-filtered using a Superose® 12 10/300 GL column (GE Healthcare, Uppsala, Sweden) equilibrated in 10 mM phosphate buffer, pH 6.5. After purification, the molar concentration of linked DM1 was assessed by UV spectroscopy, as described below.

In the modification reaction of the antibody, MAP12NP required a stronger buffer (100 mM NaH_2PO_4, 50 mM NaCl, 2 mM EDTA, pH 6.5, hereafter referred to as "Buffer B") and a longer reaction time (24 h).

2.3.2. One-step bioconjugation procedure

ADCs based on either MAL24PS (T-(L_{24}-DM1)$_3$, T-(L_{24}-DM1)$_{8–10}$), or MAP12NP (T-($cP_{(12\times2)}$-DM1)$_3$, T-($cP_{(12\times2)}$-DM1)$_7$) or MAP12PS (T-($P_{(12\times2)}$-DM1)$_3$, T-($P_{(12\times2)}$-DM1)$_8$) were prepared by the same chemical strategy, a one-step conjugation procedure as previously described [26,40]. As an example, it is here briefly reported the synthesis of T-($P_{(12\times2)}$-DM1)$_3$. To a 1.5-mL EP tube containing 78.2 μL of a phosphate buffer solution (NaCl 137 mM, KCl 2.7 mM, Na_2HPO_4 10 mM, KH_2PO_4 1.8 mM, pH 6.0), a 50 mg/mL solution of MAP12PS (3.13×10^{-4} mmol, 0.51 mg) in DMSO was gently added and mixed. Then, a small excess of DM1 (4.06×10^{-4} mmol, 0.30 mg, 50 mg/mL in DMA) was added to the linker solution. Additional 61.9 μL DMA were eventually added to have a final 50% (*v*/*v*) of organic solvent in the reaction mixture (43.5% (*v*/*v*) DMA + 6.5% (v/v) DMSO). The mixture was vortexed and incubated at 20 °C, for 1 h, under stirring at 300 rpm. The complete consumption of MAP12PS was monitored through RP-HPLC (see below). After characterization, the solution was added to a 100 mM HEPES, pH 8.0, solution containing Trs (3.47×10^{-5} mmol, 5 mg, 2.5 mg/mL). The total amount of organic solvent in the conjugation mixture was kept equal to 10% *v*/*v*. After a 2 h-incubation at 20 °C, the reaction mixture was gel-filtered using a Superose® 12 10/300 GL column (GE Healthcare, Uppsala, Sweden) installed on an AKTA® Purifier FPLC system (GE Healthcare, Uppsala, Sweden). The elution was performed under isocratic conditions in 10 mM phosphate buffer, pH 6.5, at a flow-rate of 0.5 mL/min, and monitored by registering the absorbance at 280 nm. After purification, conjugation efficiency, expressed as DAR, was determined by UV/ spectroscopy as described below. Total protein concentration was assessed through the BCA assay, using Trs as standard.

After conjugation, synthesized ADCs were dialyzed overnight at 4 °C into 10 mM Sodium Succinate buffer, 6% *w*/*v* sucrose, 0.02% *w*/*v* Tween 20, pH 5.0 (hereafter referred to as "formulation buffer") and concentrated to >10 mg/mL on a 30 kDa Vivaspin ultracentrifugation device (Sartorius, Göttingen, Germany). DAR_{UV} and protein concentration were measured at this stage as described below. Samples were then sterile filtered with Millipore 0.22 μm cellulose acetate filter (Billerica, MA, USA), snap-frozen and stored at −80 °C prior to further analysis.

2.3.3. RP-Chromatography of DM1-MAP12PS, DM1-MAP12NP, DM1-MAL24PS and DM1-SMCC

DM1-MAP12PS, DM1-MAP12NP, DM1-MAL24PS and DM1-SMCC reaction solutions were monitored through RP-HPLC analysis before the whole reaction mixture was added to the antibody solution. The analysis was committed to assessing the complete consumption of the linker by the slight excess of DM1. After 1 h of incubation at 20 °C, 2 μL of the reaction mixture were withdrawn and diluted in the starting eluting mixture to a theoretical concentration of 0.1 mg/mL in the linker. 20 μL of this solution were injected onto a Jupiter® 5 μm C18 RP-HPLC column (4.6 × 250 mm, 300 Å; Phenomenex, USA) coupled to an Agilent 1260 Infinity system (Agilent Technologies, Santa Clara, CA, USA) eluting with Milli-Q water +0.05% TFA (mobile phase A, MP_A) and ACN + 0.05% TFA (mobile phase B, MP_B). A flow-rate of 1.0 mL/min was maintained over the entire gradient as follows: 20–37% MP_B from 0′ to 2′, 37–58%-MP_B from 2′ to 22′, 58–90% MP_B from 22′ to 25%, 90–20% MP_B from 25′ to 30′. Chromatograms were registered at 220 nm and 252 nm and analyzed by using Agilent Chem Station (Agilent Technologies, Santa Clara, CA, USA). The percentage of the unreacted linker, if any, and the reaction yield (% formed product) were obtained by integrating the corresponding peaks of the chromatogram registered at 220 nm.

2.3.4. LC/ESI-MS analysis of DM1-linker reaction mixtures

To assign the identity of the species formed during the DM1-linker reactions, an LC/ESI-MS analysis was run for all the reaction mixtures. An Acquity UPLC I-Class with a Xevo G2-S QToF mass spectrometer (Waters Corp., Milford, MA, USA) was used for the analysis. The ESI source voltage was set at 3.0 kV, and the capillary temperature was set at 100 °C. The mass spectrometer was operated in positive ESI mode. After 1 h of incubation at 20 °C, as much as 10 μL of the pre-diluted reaction mixture (0.1 mg/mL theoretical linker) was injected onto an Acquity BEH300 c18 1.7 μm (2.1 × 50 mm, Waters) column using a 25-min linear gradient run at a flow rate of 0.2 mL/min, 30 °C. The gradient was programmed as follows: 37–58% MP_B from 0′ to 25′, 58–90%-MP_B, from 25′ to 30′, 90–37% MP_B from 35′ to 40′. The mobile phase A was Milli-Q water with 0.1% formic acid (MP_A) and the mobile phase B was ACN with 0.1% formic acid (MP_B).

2.3.5. Average drug-to-antibody ratio (DAR) by UV

The molar concentration of the linked DM1 was assessed by UV spectroscopy (DAR_{UV}) by exploiting the different absorbance maxima of Trs and DM1 at 280 nm and 252 nm, respectively. Since both the components absorb at the wavelengths used for the measurements, the contribution of either component at each wavelength was considered. None of the linkers had significant absorbance at these wavelengths. The equations used were the following, as reported elsewhere [19]:

$$A_{280} = \varepsilon_{Ab280}\, x\, C_{Ab} + \varepsilon_{D280}\, x\, C_D \quad (1a)$$

$$A_{252} = \varepsilon_{D252}\, x\, C_D + \varepsilon_{Ab252}\, x\, C_{Ab} \quad (1b)$$

where:

ε_{D280} = molar extinction coefficient of DM1 at 280 nm.
ε_{Ab280} = molar extinction coefficient of Trs at 280 nm.
ε_{D252} = molar extinction coefficient of DM1 at 252 nm.
ε_{Ab252} = molar extinction coefficient of Trs at 252 nm.
C_D = molar concentration of DM1.
C_{Ab} = molar concentration of Trs.

Dividing Eq. 1b by Eq. 1a and rearranging:

$$DAR = \frac{C_D}{C_A} = \frac{\varepsilon_{Ab252} - R\varepsilon_{Ab280}}{R\varepsilon_{D280} - \varepsilon_{D252}} \quad (2)$$

Where R is the total absorbance ratio (A_{252}/A_{280}). An optical path length of 10 mm is assumed by these equations. The molar extinction coefficients of the drug DM1 ($\varepsilon_{D280} = 5065\ M^{-1}\ cm^{-1}$, $\varepsilon_{D252} = 24{,}201\ M^{-1}\ cm^{-1}$) were measured experimentally in our laboratories. As for Trs, the values of the extinction coefficients were as follows: $\varepsilon_{Ab280} = 215{,}380\ M^{-1}\ cm^{-1}$, as estimated using the ExPASy ProtParam tool, and $\varepsilon_{Ab252} = 79{,}990\ M^{-1}\ cm^{-1}$, as measured experimentally in our laboratories.

Spectra were taken on a single-beam Thermo Scientific Evolution 201 spectrophotometer (Waltham, MA, USA). Samples were diluted to approximately 0.5 mg/mL in either 10 mM phosphate buffer, pH 6.5, or formulation buffer. A blank was recorded with the same buffer and measurements were performed at ambient temperature.

2.3.6. Evaluation of isomeric distribution of ADCs by ESI-QToF mass analysis

Mass analysis of intact and deglycosylated ADCs was performed using a Xevo G2-S QTof mass spectrometer (Waters Corp., Milford, MA, USA), operating in positive ion mode. Before analysis, deglycosylated samples were obtained as follows: 1 μL of PNGase (500 units, 5000 units/mg of antibody; New England Biolabs, Ipswich, MA, USA) was added to a solution of 100 mM Tris-HCl, pH 7.5, containing 100 μg of ADC (≥ 1 mg/mL) and incubated overnight at 37 °C with stirring. Following deglycosylation, the sample was buffer exchanged into 150 mM ammonium acetate, pH 7.4 by using a 30 kDa Vivaspin ultracentrifugation device (Sartorius, Göttingen, Germany). Then, the sample (10 μL, ~0.3 mg/mL) was directly introduced into the mass spectrometer. The optimized instrument conditions were the following: capillary voltage of 2.5 kV, sampling cone voltage of 40 V, desolvation temperature of 450 °C and source temperature of 120 °C. The recorded mass spectra were deconvoluted using the maximum entropy MaxEnt™ algorithm on MassLynx 4.1 (Waters, Milford, MA, USA), after background subtraction (polynomial order 25, 10% area beneath the curve), with a minimum intensity ratio of 30% (left and right). The resolution (Da/channel), the deconvolution range, and width at half height were adjusted for each spectrum to gain more sensitivity.

The average DARs (DAR_{MS}) were calculated based on the relative peak area of each DAR species in the deconvoluted spectrum divided by the total peak area of that sample. The summation of the product of each DAR species multiplied by its relative peak area gave the average DAR value (Eq. 3).

$$\text{Avg DAR}_{MS} = \sum_{i=DAR\ min}^{DAR\ max} (DAR_i x\ Relative\ Peak\ Area_{DARi_i}) = \sum_{i=DAR\ min}^{DAR\ max} \left(DARi\ x\ \frac{Peak\ Area_{DARi_i}}{Total\ Peak\ Area} \right) \quad (3)$$

DAR_{MS} measurement assumes equal ionization efficiency between various DAR species of the ADC.

Unconjugated linker fraction (UL_{fxn}) relative to the total linker content was calculated from the deconvoluted mass spectrum, as previously reported [41]. A weighted area for each peak was calculated based on the number of linkers it contained (both with and without conjugated drug).

$$Wt\ Area_{total\ linker} = (Number\ of\ linkers) \times (Peak\ Area) \quad (4)$$

For each peak with the unconjugated linker, a weighted area of the unconjugated linker is calculated.

$$Wt\ Area_{unconjugated\ linker} = (Number\ of\ unconjugated\ linkers) \times (Peak\ Area) \quad (5)$$

Therefore, for the entire mixture of species, the unconjugated linker fraction was calculated by

$$UL_{fxn} = \Sigma Wt\ Area_{unconjugated\ linker} / \Sigma Wt\ Area_{total\ linker} \quad (6)$$

2.3.7. MALDI-ToF MS analysis

As much as 1 μL of desalted Trs or ADC of interest was mixed with 1 μL of a saturated solution of sinapinic acid in 0.1% TFA in ACN/water (50:50, *v*/v). The resulting mixture was spotted on the MALDI target and it was left to dry in the air. Then 1 μL of the matrix solution was added to

each spot and it was left to dry again. Mass spectra were obtained using a MALDI spectrometer with a REFLEX time-of-flight (4800 Plus MALDI TOF/TOF, AB Sciex, Framingham, MA, USA) equipped with a SCOUT ion source, operating in positive linear mode. A pulsed UV laser beam (nitrogen laser, λ 337 nm) generates ions that are accelerated to 25 kV.

2.4. Stability study

Upon thawing, the antibody concentration of the test samples was measured again. Samples were diluted to 8–10 mg/mL with the formulation buffer, transferred in sterile glass vials and placed in a Stability Test Chamber at 40 °C, 60% humidity for 4 weeks. Fresh aliquots of Trs (Herceptin®, 21 mg/mL) and Kadcyla® (20 mg/mL) were thawed and simply diluted to 10 mg/mL with formulation buffer in sterile conditions right before being thermally stressed. At every time point (0 d, 7 d, 14 d, 21 d, 28 d), 60 μL of each test sample was collected in sterile conditions and equally distributed among the different analyses conducted in the stability study.

2.4.1. Evaluation of aggregates by size exclusion chromatography (SEC)

The Agilent 1290 UHPLC system (Santa Clara, CA, USA) with the TSKgel® UP-SW3000 column (phase diol, 4.6 × 300 mm, 2 μm; Tosoh Bioscience, Japan) was used to detect antibody aggregation/degradation products by hydrodynamic volume, evaluate the DAR of the monomer (DAR_{SEC}) and estimate the molecular weight of aggregating species and degradants. The mobile phase was composed of 0.1 M Na_2SO_4, 0.05% (*w/v*) NaN_3 in 0.1 M phosphate buffer, pH 6.7. In the case of T-(MCC-DM1)$_3$, T-(MCC-DM1)$_7$, T-(*c*P$_{(12\times2)}$-DM1)$_3$ and T-(*c*P$_{(12\times2)}$-DM1)$_7$, the mobile phase contained 7.5% (*v/v*) 2-propanol (IPA). At every time point, the collected aliquot (60 μL) was centrifuged (10,000 ×*g* for 1 min), and 8 μL of the upper solution (8–10 mg/mL) were injected onto the column at a flow rate of 0.35 mL/min. In the case of T-(MCC-DM1)$_3$, T-(MCC-DM1)$_7$, T-(*c*P$_{(12\times2)}$-DM1)$_3$ and T-(*c*P$_{(12\times2)}$-DM1)$_7$, a flow rate of 0.25 mL/min was maintained during the analyses and 2–3 μL were injected onto the SEC column. Absorbance was detected at both 280 nm and 252 nm. The series of test samples were injected on the same day of every withdrawal along with a set of MW standards (1. Dextran blue; 2. Apoferritin; 3. BSA dimer; 4. BSA monomer; 5. Ovalbumin; 6. RNase A; 7. GYG).

Chromatograms generated by using Agilent Chem Station (Agilent Technologies, Santa Clara, CA, USA) allowed for direct relative quantification of soluble aggregates, if any, as well as an estimation of the DAR_{SEC} by integrating the monomer peak in the 252 and 280 nm channels.

2.4.2. Unconjugated drug analysis

As much as 10 μL of each ADC solution was diluted to 100 μL with formulation buffer. Protein fraction was precipitated by treating the ADC solution with four-fold the volume of cold (−20 °C) acetone and 2 h-incubation at −20 °C. After centrifugation, the supernatant was recovered and reduced in volume under vacuum. The solid residue was dissolved in 50 μL 63% H2O + 0.05% TFA – 37% ACN + 0.05% TFA. 20 μL of this solution was injected onto a Jupiter® C18 300 Å column (4.6 × 250 mm, 5 μm, Phenomenex, USA) at a flow rate of 1.0 mL/min. The gradient was programmed as follows: 37–58% MPB from 0′ to 25′, 58–90%-MPB, from 25′ to 30′, 90–37% MPB from 35′ to 40′. Free DM1-related species were quantified using a standard curve generated with serial dilution of DM1 standard stock solution. The content of the unconjugated drug-related species at each time point was calculated as a fractional value of the total drug of the unstressed ADC solution, as follows:

$$Free\ DM1\% = moles\ of\ free\ DM1/(DAR \times moles\ Trs) \quad (8)$$

2.4.3. SDS-PAGE

Reducing and non-reducing SDS-PAGE with Coomassie blue stain were used to detect covalent aggregates and degradation species and discriminate between reducible and non-reducible aggregates. The runs were performed using Mini-PROTEAN® TGX™ precast gels (4–15% acrylamide) and a constant voltage of 250 V (starting current: 60 mA). At every time point, 5 μL of the collected aliquot were withdrawn and diluted to 1 mg/mL in Milli-Q water. Then 7.5 μL of this solution were mixed with 7.5 μL of reducing (β-ME-containing) or non-reducing loading buffer, before sample denaturation at 100 °C for 3 min. 5–10 μg of antibody were eventually loaded on the gel.

2.5. In vivo pharmacokinetics in BALB/C mice

Female BALB/c mice (weight 20–29 g) were injected *via* a lateral tail vein with 10 mg/kg (Trs equivalents) of different ADCs (eighteen mice per group) The withdrawn schedule (2′, 30′, 2 h, 4 h, 8 h, 1 d, 2 d, 3 d, 5 d, 7 d, 10 d, 14 d, 21 d, 28 d) was obtained combining different animals. A blood sample (~70 μL) was withdrawn from the submandibular cheek, collected in heparinized EP tubes, and processed to plasma after centrifugation at 1500 ×*g* for 15 min. Plasma samples were stored at −80 °C until further analysis.

The total antibody concentration was determined by employing a 96-well anti-human IgG1 ELISA kit (Abcam, Cambridge, UK) that is pre-coated with a mouse monoclonal anti-human Fc antibody as a capture antibody. Standards or samples diluted in the assay diluting buffer were added to the pre-coated 96-well plates. After a 2.5-h incubation, plates were washed, and the detection antibody (polyclonal goat anti-human Fab antibody) was added for an additional 2 h. The plates were washed again and incubated with HRP-streptavidin for 45 min.

After an additional wash, tetramethyl benzidine substrate (TMB) was added for color development. The reaction was stopped after 30 min by the addition of 1 M phosphoric acid. Plates were read on Bio Tek EL311SX Microplate Autoreader Automated (Vinooski, VT, USA) at a wavelength of 450 nm. Total Trs concentration was extrapolated from a power-fit of the standard curve. The data were further fit to a two-compartment model to derive the PK parameters using PKSolver® [42].

3. Results

3.1. Preparation and preliminary characterization of the ADCs

The manufacturing of Kadcyla® involves a two-step process, where Trs is reacted with SMCC in step 1 to yield the intermediate T-MCC conjugate, followed by reaction of T-MCC and the thiol-bearing DM1 in step 2 to yield a stable thioether-bond with the maleimide moieties [21,43]. We first evaluated the potential applicability of this synthetic strategy by preparing T-(L$_{24}$-DM1)$_3$, T-(*c*P$_{(12\times2)}$-DM1)$_3$, and T-(MCC-DM1)$_3$. Linkers were chosen to address three distinct variables: (1) presence or absence of PEG, (2) configuration of the PEG molecule (linear or pendant), and (3) nature of functional group reacting with the antibody.

In the first step, the OSu ester or *p*NP carbonate side of the linker were randomly reacted with lysine residues in Trs under slightly acidic conditions (pH 6.5), resulting in the displacement of the two above-mentioned groups to give an amide and a carbamate linkage at the mAb lysine residues, respectively (Fig. 2a). Acidic conditions were chosen to prevent the hydrolysis of both the OSu ester and *p*NP carbonate groups and the maleimide moiety at the other side of the linker, as well as to limit the reactivity of the lysine ε-amino group towards the maleimide ring. The pendant linker MAP12NP was more refractory than the linear counterpart MAL24PS, as shown by a comparison of the linker excess per antibody and the incubation time in Table 1. This is consistent either with the steric hindrance the pendant PEG chains might create around the *p*NP carbonate bioconjugation group or with an inbuilt reduced reactivity of the *p*NP carbonate group in the conditions employed. The absence of the PEG molecule in the SMCC linker drove to better modification efficiency (Table 1).

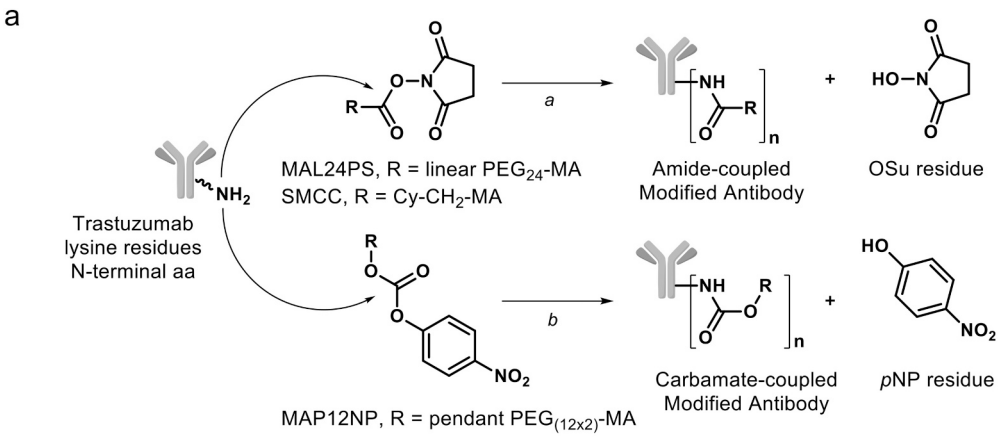

[a] 50 mM phosphate buffer, pH 6.5, 4h, r.t. stir. for MAL24PS and SMCC
[b] 100 mM phosphate buffer, pH 6.5, 20h, r.t. stir. for MAP12NP.

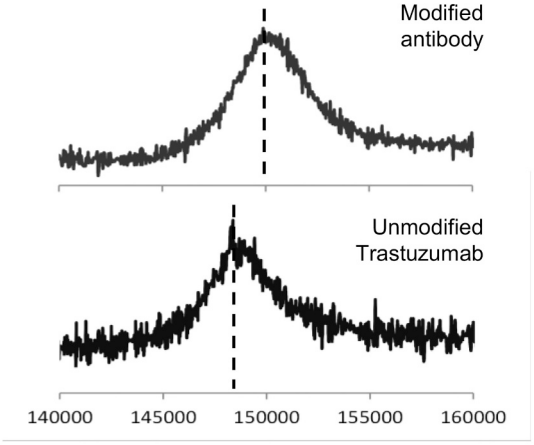

Modified antibody	Mass (Da)	LAR[a]
T-MAL24PS	153947.2 Da	4.24
T-MCC	149854.4 Da	6.10
T-MAP12NP	155488.0 Da	4.89

[a] Found mass of the modified antibody subtracted from the found mass of trastuzumab (148511.1 Da) and divided by the molecular weight of the linker (lacking either the OSu group (115 Da) or *p*NP group (139 Da)).

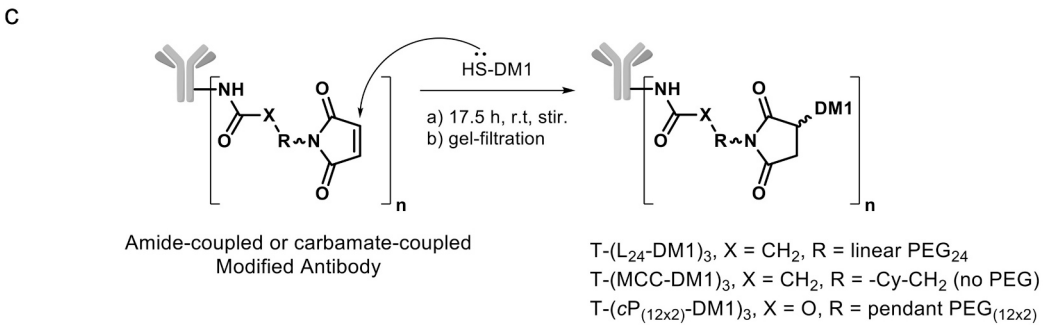

Fig. 2. Process flow for the preparation of the ADCs from Trs *via* the two-step conjugation procedure. a) Modification reaction of the antibody; b) Illustrative MALDI-ToF MS analysis and linker-to-antibody ratios (LARs) for the modified antibodies; c) Conjugation reaction with the sulfhydryl of the DM1 drug.

The rate of modification – referred to as linker-to-antibody ratio or LAR in Table 1 – was measured by evaluating the mass shift from the unconjugated antibody in MALDI-TOF mass analysis (Fig. 2b). The average number of incorporated linkers was important to assess the amount of DM1 required for the conjugation step.

In the conjugation step, an excess (1.7 equiv./linker) of the thiol-bearing DM1 was hence reacted with the maleimide moieties of the modified antibody in a classical Michael-type addition reaction to obtain the final conjugates (Fig. 2c). A 10 mg/mL stock solution of DM1 in DMA was slowly added to the modified antibody solution, making sure that the total amount of DMA in the conjugation mixture was kept below 6% (*v*/*v*). After a 17.5 h-incubation followed by Fast Protein Liquid Chromatography (FPLC) to remove the excess DM1, the ADCs were characterized by UV/Vis spectroscopy to determine the average DAR.

Despite the 1.7-fold molar excess of DM1 per linker used in the conjugation step, the long incubation time, and the well-known efficiency of the thiol/maleimide chemistry, the high LAR/DAR ratios (≥ 1.2, Table 2) suggest that the conjugation of DM1 was not complete, and part of the incorporated linkers had remained unreacted in the final conjugates.

These unconjugated linker-modified antibody species were identified as secondary less abundant series of peaks in the ESI-QToF mass

Table 1
Modification step of the two-step conjugation procedure. A comparison of the linkers is provided as far as the linker structure, the incubation time with Trs, the linker excess per antibody, the LAR value, and the efficiency of modification.

Linker name	PEG structure	Time (h)	Linker/Trs reaction molar ratio[a]	LAR[a]	% ME[b]
MAL24PS	Linear PEG_{24}	4	10.5	4.24	40.4
SMCC	No PEG	4	7.0	6.10	87.1
MAP12NP	Pendant $PEG_{(12\times2)}$	24	60	4.87	8.1

[a] Linker-to-antibody ratio, measured experimentally by MALDI-TOF MS as reported in Fig. 2.
[b] Modification efficiency, calculated from LAR / (linker/Trs) × 100.

Table 2
Conjugation efficiency expressed as LAR/DAR ratio. The ADCs obtained by the two-step procedure have a fraction of linkers not conjugated to DM1 but appended on the antibody, as indicated by the LAR values being higher than the DAR values.

ADC	PEG structure	LAR[a]	DAR[b]	LAR / DAR[c]
T-$(L_{24}$-DM1$)_3$	Linear PEG_{24}	4.24	3.67	1.2
T-(MCC-DM1$)_3$	No PEG	6.10	3.81	1.6
T-$(cP_{(12\times2)}$-DM1$)_3$	Pendant $PEG_{(12\times2)}$	4.87	3.55	1.4

[a] LAR, measured experimentally by MALDI-TOF MS as reported in Fig. 2.
[b] DAR, measured experimentally from UV spectroscopy and eq. (1).
[c] Conjugation efficiency, calculated as LAR / DAR ratio

deconvoluted spectra of the ADCs. Fig. 3a shows the deconvoluted spectrum of T-$(L_{24}$-DM1$)_3$ ADC, where there is evidence of species containing one unconjugated linker (labeled as $D_n + 1$ L in the figure). It can be noted how these species follow their own distribution and are equally spaced among each other and from the main DAR distribution. The observed average offset of 1290 Da between the two distributions correlates well to the predicted mass of MAL24PS bound to the antibody but lacking DM1 (1280 Da). Similar results were obtained with T-(MCC-DM1$)_3$ where species bearing up to three unconjugated linkers could be found in the deconvoluted spectrum (Fig. 3b, * for 1 linker, ** for 2 linker and *** for 3 linkers). In this case, each distribution has masses ~220 Da higher than the preceding set of peaks in the spectrum. Each of these peaks corresponds to a drug-loaded species that also contains one to three MCC linkers (219 Da) that have not reacted with DM1 in the conjugation step. The level of unconjugated linker-modified antibody species (UL_{fxn}) was estimated to be approximately 19% and 49% in T-$(L_{24}$-DM1$)_3$ and T-(MCC-DM1$)_3$, respectively. Under the experimental conditions employed, the deconvoluted spectrum of Kadcyla® also revealed that ~9% of the total linker species bound to the antibody did not have a conjugated DM1, in line with what is found in the literature [41,44,45] (Fig. S1). Therefore, it seems that the presence of unconjugated linker-modified ADC species is an inevitable consequence of the two-step conjugation procedure, regardless of the presence of a PEG molecule in the linker structure, or the configuration assumed by the PEG molecule, or the nature of the antibody-linker linkage. It might be that once appended on the antibody, the maleimide heads end in chemical surroundings that are less accessible to the thiol reagent. Furthermore, it is not ruled out that some of the introduced maleimides might react with proximal lysine residues of the antibody leading to covalent cross-linking between mAb peptide chains, as it was demonstrated for Kadcyla® [41].

To overcome this issue, we decided to pursue a "one-step bioconjugation" strategy that involved the direct conjugation of the antibody with pre-conjugated drug-linker species. To this effect, the linker-drug products DM1-MAL24PS, DM1-SMCC, DM1-MAP12PS, and DM1-MAP12NP were first synthesized in a reaction scheme where the thiol-bearing DM1 reacts with the maleimide moiety of the linker (MAL24PS, SMCC, MAP12PS, and MAP12NP) under mildly acidic conditions following a Michael addition reaction (Fig. 4a). In each case, the reaction progress was followed by RP-HPLC. Fig. 4b shows a typical set of peaks obtained upon 1 h-incubation of each linker with excess DM1; the identity of the chemical species present in each fraction was confirmed by LC-MS (SI). In all cases, the most abundant species were represented by the DM1-linker thioether addition product, as determined by the relative percentage calculated by the integrated peak area, and there was no evidence of free unreacted linker after 1 h-incubation. Hydrolysis of OSu ester or *p*NP carbonate groups on the DM1-linker occurred but only at low rates under these conditions. Traces of by-products in which DM1 had also reacted at the OSu ester or *p*NP carbonate side on the linker were also detected. The thioether addition products (DM1-MAL24PS, DM1-SMCC, DM1-MAP12PS, and DM1-P12NP), their hydrolyzed forms (DM1-MAL24-COOH, DM1-SMCC-COOH, DM1-MAP12-COOH, and DM1-MAP12-OH), and the thioester- or thiocarbonate-thioether by-products (DM1-L24-DM1, DM1-P12-DM1, and DM1-P12-DM1 (SOCO)) eluted as pairs of peaks in RP-HPLC as a result of the two diastereomers on the neosuccinimide ring, which was verified by the equivalence of masses determined from LC-MS of the two different peaks (Supplementary Fig. S2 and Supplementary Table 1).

Initial attempts to isolate the DM1-linker addition products DM1-MAL24PS, DM1-MAP12PS, and DM1-MAP12NP by flash silica chromatography or semi-preparative RP-HPLC were not successful as the purifications were accompanied either by the loss of the OSu moiety on

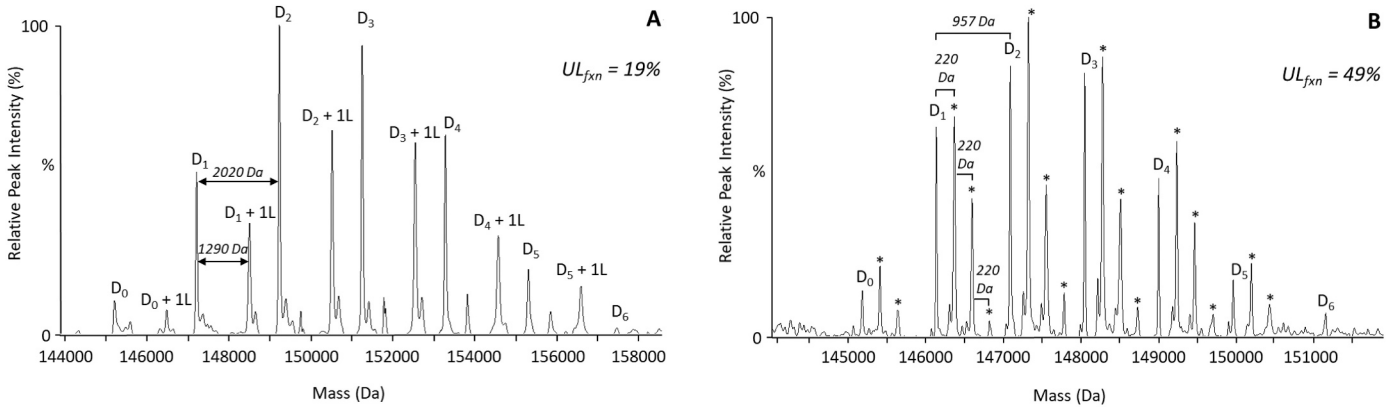

Fig. 3. Illustrative ESI-QToF MS deconvoluted spectra of a) T-$(L_{24}$-DM1$)_3$ and b) T-(MCC-DM1$)_3$. a) The deconvoluted spectrum of T-$(L_{24}$-DM1$)_3$ highlights the presence of a secondary less abundant distribution of peaks – identified as $D_n + 1$ L – in addition to the main DAR distribution. The two series for each DAR are separated by an average offset of +1290 Da; b) The deconvoluted spectrum of T-(MCC-DM1$)_3$ highlights as many as three distributions additional to the main DAR distribution (starred peaks). These series of peaks are separated from each other by an offset of approximately +220 Da.

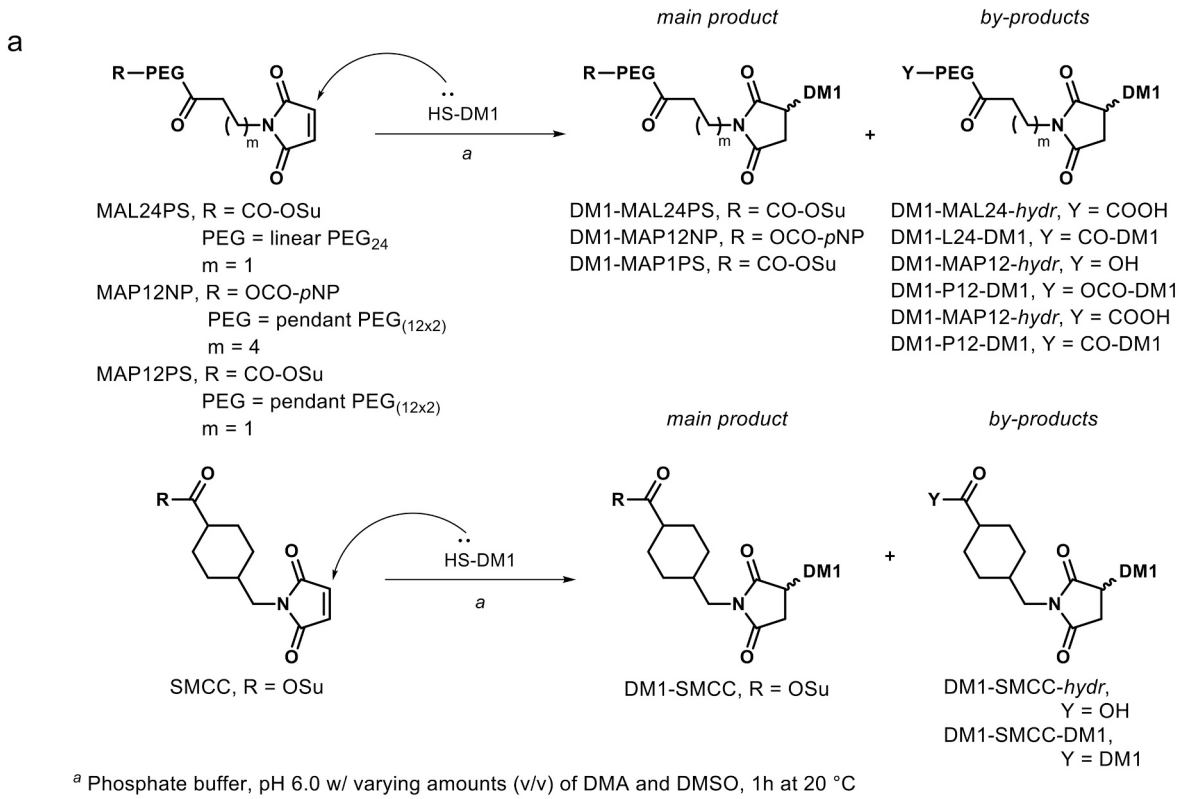

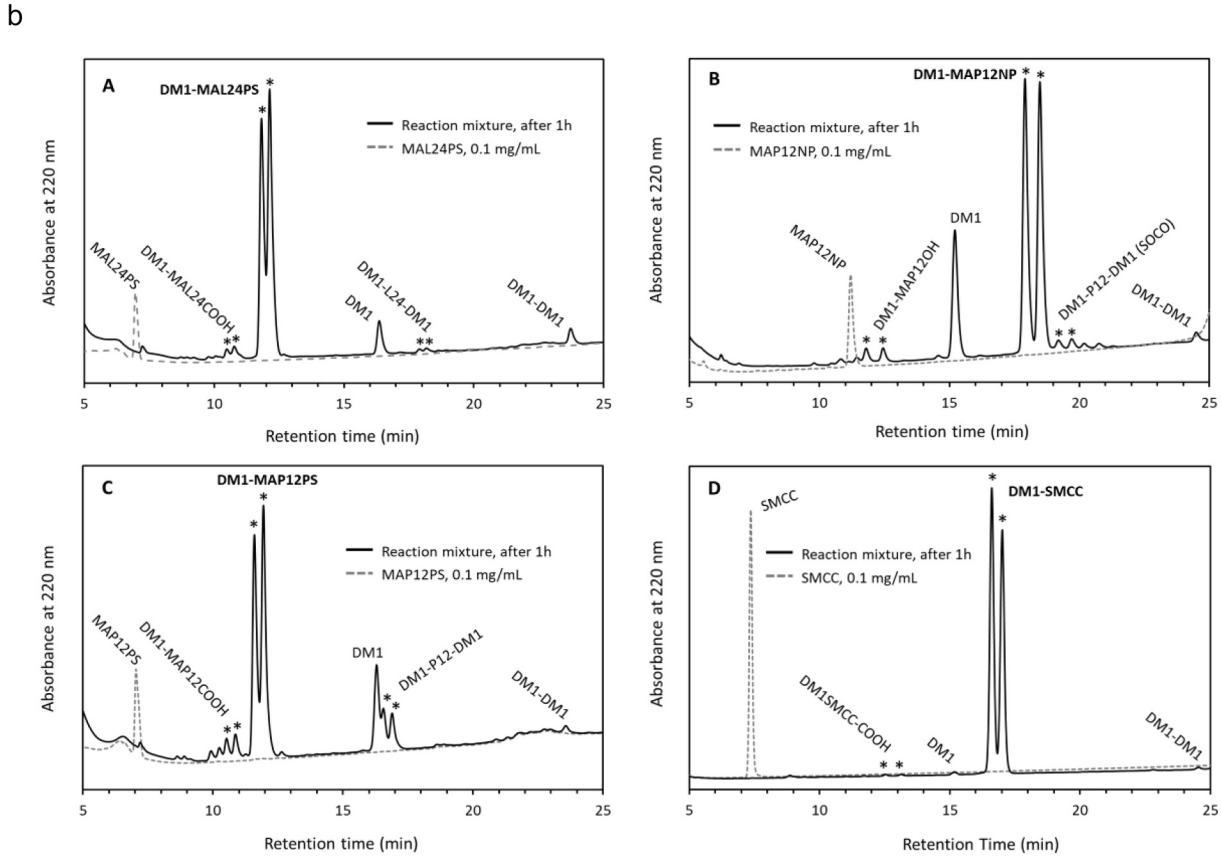

Fig. 4. a) Michael addition reactions of MAL24PS, SMCC, MAP12NP, and MAP12PS with excess DM1 to yield the desired DM1-linker thioether addition products plus by-products; b) RP-HPLC chromatograms of the thiol-ene reaction of the linkers and excess DM1 after 1 h-incubation at 20 °C. Gradient A was used in runs A and C, gradient B was used in runs B and D. The asterisks (*) indicate the diastereomers. The species DM1-SMCC-DM1 in chromatogram D (Rt = 26.9 min and 27.1 min) is not reported within this zoom.

the linker or the prevalence of one or the other diastereomer in the pure product (data not shown). Therefore, the thioether addition products DM1-MAL24PS, DM1-MAP12PS, and DM1-MAP12NP were used directly without isolation for the conjugation with Trs. The mAb was expected to react only with the DM1-linker species having the antibody-reactive moiety (*i.e.*, OSu ester or *p*NP carbonate) in place, thereby neglecting the presence of the other drug-linker by-products present in the medium (*i.e.*, hydrolyzed DM1-linker species, DM1-linker-DM1 species). In this strategy, the generation of the DM1-linker thioether addition products and the subsequent conjugation with Trs can hence be considered as the two steps of the same reaction, separated by no interim purification. Depending on the target DAR intended to be reached finally, the equivalents of linker per Trs were changed accordingly (Table 3).

Upon completion of the Michael addition of the linkers with DM1 (as determined by RP-HPLC), the whole reaction mixtures were therefore added to the antibody solution in a basic buffer (pH 8.0), resulting in random conjugation to the antibody lysine residues (Fig. 5). The conjugation of DM1-MAP12NP to Trs required more excess of linker per antibody as well as longer incubation times than the other linkers (Table 4). Since the conversion to the addition product with DM1 is similar for all the linkers (Table 3), the low conjugation efficiency, shown by DM1-MAP12NP, has to be related to the low reactivity of the *p*NP carbonate group, as already highlighted in the two-step conjugation procedure (Table 1). The steric hindrance hypothesis can be here ruled out as the other DM1-linker bearing two pendant PEG_{12} chains, DM1-MAP12PS, showed good conjugation efficiency (Table 4).

ADCs obtained by this "one-step bioconjugation" strategy showed, by Esi-QTof mass analysis, a usual symmetrical binomial distribution with no evidence of sub-populations with unconjugated linkers grafted on the antibody (Fig. 6). DAR species could be easily identified, and the mass shift matched the predicted mass of the linker-payload bound to the antibody. Interestingly, the mean DARs measured from the MS data (Eq. 3) sufficiently correlated with those determined by conventional UV spectroscopy, suggesting a good recovery of all the species from the full charge envelope of the ionized products. In the case of the high-DAR PEGylated ADCs T-$(L_{24}$-DM1$)_8$, T-$(cP_{(12\times2)}$-DM1$)_7$, and T-$(P_{(12\times2)}$-DM1$)_8$, the drug distribution in the deconvoluted spectra shifted to higher masses, and ADC isomers with a DAR < 2, including the naked antibody, were completely absent. In a separate experiment, we spiked a sample of a DAR_{MS} 5.0 deglycosylated PEGylated ADC with 1 μg (~1%) of deglycosylated naked Trs and analyzed the mixture. The deconvoluted mass spectrum of the spiked sample showed the peak corresponding to the naked antibody (D_0), which was absent in the non-spiked sample (Supplementary Fig. S3). The appearance of the new peak due to the addition of 1% naked Trs suggests that, even in a DAR 5 ADC, only a very small portion, if any, of naked antibody is present in the ADC mixture, and that is significantly less than 1%.

Unlike the PEG-linkers, the purification of DM1-SMCC by flash-silica chromatography was successful, presumably thanks to a lighter interaction of SMCC with SiO_2 than the PEG-linkers. Once the Michael addition reaction was completed, as determined by TLC and RP-HPLC (Supporting Fig. S4), the crude product DM1-SMCC was purified through flash chromatography (eluting system: 96:4 DCM/EtOH). ^{1}H NMR and ESI-MS analyses were used to confirm the product (Supporting Fig. S4). For the conjugation with the antibody, the 20-mM stock solution of the pure product DM1-SMCC in DMA needed to be added to the antibody solution slowly while stirring; a gentle agitation through a small magnetic stirring bar resulted to be key to avoid precipitation upon adding. When targeting low DARs, no precipitation occurred either upon adding or during the 20 h-incubation with Trs, and T-(MCC-DM1)$_3$ was obtained with decent conjugation efficiency and good mAb recovery (Supplementary Table 2). The high-DAR sample T-(MCC-DM1)$_7$ was also obtained with acceptable recovery in mAb and acceptable conjugation efficiency (Supplementary Table 2). Mean DARs above 7 were almost inaccessible with the SMCC linker because of profuse antibody precipitation during the conjugation reaction (Supplementary Table 2). Pleasingly, mass analysis of T-(MCC-DM1)$_3$ confirmed the absence of linkers bound to the antibody but not conjugated to DM1 (Supporting Fig. S5). Mass spectra of T-(MCC-DM1)$_7$ could not be obtained due to precipitation issues of the samples during the deglycosylation protocol – either during the overnight incubation at 37 °C or the sample desalting with 30 kDa molecular weight cut off (MWCO) centrifugation devices.

Table 3
Conditions of the Michael addition reactions of MAL24PS, MAP12NP and MAP12PS with excess DM1 to generate the DM1-thioether addition products.

Linker name[a]	% organic solvent (*v*/*v*)	Linker equiv. /Trs	DM1 equiv./ linker	% conversion to DM1-linker[b]	Target DAR (range)
MAL24PS	44.5% DMA + 5.5% DMSO	6.3	1.4	91.3	3–4
	23.2% DMA + 5.7% DMSO	20	1.3	86.6	7–8
MAP12NP	41.9% DMA + 6.2% DMSO	24	1.3	85.3	3–4
	16.8% DMA + 6.3% DMSO	50	1.4	84.7	7–8
MAP12PS	43.5% DMA + 6.5% DMSO	7.5	1.3	74.9	3–4
	43.4% DMA + 6.6% DMSO	18	1.3	72.9	7–8

[a] Each linker has two different conditions depending on the final target DAR (see text).
[b] Relative percentage calculated by the integrated peak area of the Michael addition product in the RP-HPLC chromatogram.

3.1.1. Stability study

The physical stability of the ADCs was investigated by both SEC-UPLC and SDS-PAGE to have a comprehensive picture of the possible aggregation species. Instead, reverse phase chromatography was committed to characterizing and quantifying free drug or drug-related impurities that might have been generated because of chemical instability issues on either the drug side, or the antibody side.

By using SEC, we followed the aggregation and degradation propensity under thermal stress of the PEGylated ADCs obtained by the "one-step" bioconjugation procedure (T-$(L_{24}$-DM1$)_3$, T-$(L_{24}$-DM1$)_8$, T-$(cP_{(12\times2)}$-DM1$)_3$, T-$(cP_{(12\times2)}$-DM1$)_7$, T-$(P_{(12\times2)}$-DM1$)_3$, T-$(P_{(12\times2)}$-DM1$)_8$) compared to Trs, Kadcyla®, and the in-house Kadcyla® analogs prepared in our laboratories (T-(MCC-DM1)$_3$ and T-(MCC-DM1)$_7$).

It is worth noting that the extent of aggregation for the unconjugated Trs remained low and relatively constant over 4 weeks (~ 0.5%, Fig. 7a), disclosing a strong resistance of the antibody *per se* against aggregation phenomena, as reported elsewhere [21]. Conversely, the thermal stress of the marketed Kadcyla®, T-(MCC-DM1)$_3$ and T-(MCC-DM1)$_7$ resulted in a higher formation of aggregates, leading to a final aggregate content of 4.2%, 4.8%, and 16%, respectively (Fig. 7a). These results suggest that the conjugation of the moiety SMCC-DM1 to Trs renders the antibody more prone to aggregation as demonstrated in previous studies [21,45]. If the non-PEGylated SMCC linker is still able to cope with low drug loads (3–4), it cannot certainly be exploited on Trs-DM1 ADCs for high-drug load delivery. The introduction of a PEG unit within the linker structure produced a different effect depending on the positioning of the

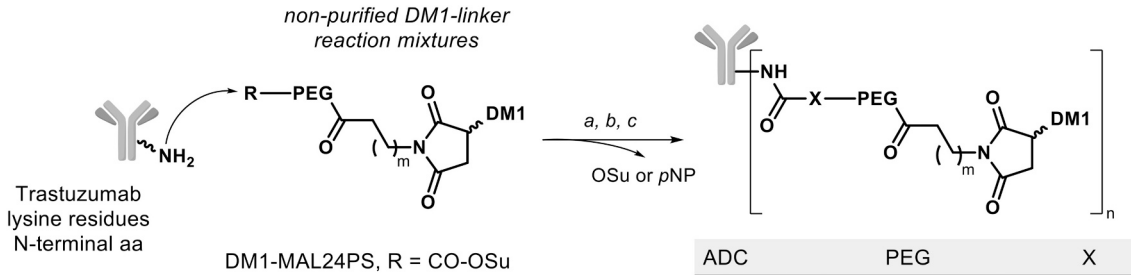

DM1-MAL24PS, R = CO-OSu
PEG = linear PEG_{24}
m = 1
DM1-MAP12NP, R = OCO-*p*NP
PEG = pendant $PEG_{(12x2)}$
m = 4
DM1-MAP12PS, R = CO-OSu
PEG = pendant $PEG_{(12x2)}$
m = 1

ADC	PEG	X	m	n
T-$(L_{24}$-DM1$)_3$	linear PEG_{24}	CH_2	1	3
T-$(L_{24}$-DM1$)_8$	linear PEG_{24}	CH_2	1	8
T-$(cP_{(12x2)}$-DM1$)_3$	pendant $PEG_{(12x2)}$	O	4	3
T-$(cP_{(12x2)}$-DM1$)_7$	pendant $PEG_{(12x2)}$	O	4	7
T-$(P_{(12x2)}$-DM1$)_3$	pendant $PEG_{(12x2)}$	CH_2	1	3
T-$(P_{(12x2)}$-DM1$)_8$	pendant $PEG_{(12x2)}$	CH_2	1	8

[a] 100 mM HEPES buffer, pH 8.0 w/ 10% (v/v) DMA+DMSO, 2h at 20 °C
[b] Gel - filtration (Superose, GE; phosphate buffer, pH 6.5)
[c] Dialisys into 10 mM succinate, pH 5.0, w/ 6% (w/v) sucrose, 0.02% (w/v) tween 20

Fig. 5. Conjugation reactions of trastuzumab with DM1-linker reaction mixtures to yield the desired ADCs. Solutions containing the DM1-linker thioether addition products were added directly to the antibody solution (100 mM HEPES, pH 8.0).

Table 4
Conditions of the conjugation reactions with Trs and conjugation efficiency expressed as a function of DAR_{UV} of the final ADCs and the efficiency of the DM1-linker reactions.

ADC	Antibody-linker bonding	Drug-linker/Trs[a]	Incubation time (h)	DAR_{UV}[b]	% CE[c]
T-$(L_{24}$-DM1$)_3$	-HN-C(=O)-R	5.7	2	3.4	59.1
T-$(L_{24}$-DM1$)_8$	-HN-C(=O)-R	16.5	2	7.5	45.5
T-$(cP_{(12\times2)}$-DM1$)_3$	-HN-C(=O)-OR	21.3	24	3.7	17.4
T-$(cP_{(12\times2)}$-DM1$)_7$	-HN-C(=O)-OR	42.3	24	7.3	17.2
T-$(P_{(12\times2)}$-DM1$)_3$	-HN-C(=O)-R	5.6	2	3.4	60.8
T-$(P_{(12\times2)}$-DM1$)_8$	-HN-C(=O)-R	15.3	2	8.0	52.2

[a] Calculated stochiometric ratios based on the % conversion of the linker to the DM1-linker thioether addition product (see Table 3).
[b] Measured drug-to-antibody ratio by UV spectroscopy.
[c] Conjugation efficiency, calculated from DAR_{UV} / (drug-linker/Trs) × 100.

polymer as well as the DM1 loading. The low aggregation tendency of the pendant carbamate-coupled ADCs T-$(cP_{(12\times2)}$-DM1$)_3$ and T-$(cP_{(12\times2)}$-DM1$)_7$ was counterbalanced by a profuse chemical instability as will be discussed later, so these samples are not included in the following discussion. At low DARs, a linear 24-unit PEG molecule and two 12-unit pendant PEG molecules seemed to be both beneficial to the stability of the conjugates as ADCs T-$(L_{24}$-DM1$)_3$ and T-$(P_{(12\times2)}$-DM1$)_3$ showed only minimal aggregation levels within the study (0.6% and 0.5%, respectively, at the end of the study, Fig. 7a). At DAR 7–8, the pendant ADC T-$(P_{(12\times2)}$-DM1$)_8$ remained mainly monomeric (> 96% at t28, Fig. 7a and Fig. 7b, chromatogram C) and with small amounts of aggregates (HMW1 and HMW2 in chromatogram D, Fig. 7b, slowly increasing to an overall content of 2.99% at t28, Fig. 7a) and fragments (LMWS in chromatogram D, Fig. 7b, slowly increasing to a final content of 1.42%, Fig. 7a) after 4 weeks. Conversely, the linear conjugate T-$(L_{24}$-DM1$)_8$ showed evident monomer depletion during the study (~11% at t28; note the inset in chromatogram A, Fig. 7b) and the concomitant formation of two distinct aggregating species, HMW1 and HMW2 (chromatogram B, Fig. 7b). Although the aggregate peaks together grew to acceptable levels after 4 weeks (~3.8%, Fig. 7a), the growth profile of the two, and especially of the earlier eluting HMW1, may be indicative of a stronger tendency to aggregation (note the difference with the same aggregate peak HMW1 of the pendant conjugate in chromatogram D). Furthermore, the mismatched values of the final aggregate content and the final monomer content in the conjugate may be reflective of additional routes that lead to monomer loss such as protein adsorption on the vial surface following partial protein unfolding and exposition of hydrophobic sites. Degradation and denaturation phenomena might also have contributed to reducing the monomer content in T-$(L_{24}$-DM1$)_8$, but the extensive broadening and tailing of the monomer peak prevented an accurate quantification of the hydrodynamically smaller fragments (*i.e.*, LMWs) present in the solution.

To disclose further changes of the ADC composition over time, the average DAR of the monomer peak on the SEC chromatogram was calculated using the UV absorbance at each peak maximum. A DAR decrease of the monomer peak was observed for all the ADCs object of this study, including Kadcyla® (Fig. 8). It is reasonable to suppose that the more conjugated species forming the ADCs (*i.e.*, DAR 6–8 species in ADCs with average DARs of 3–4, and DAR 11–13 species in ADCs with average DARs of 7–8), being more prone to aggregation, will progressively forsake the mixtures, which will consequently become DM1 impoverished over time. The DAR loss is therefore proportional to the DAR of the species aggregating such that high-DAR ADCs have higher DAR reduction. ADC T-$(P_{(12\times2)}$-DM1$)_8$ (grey circles in Fig. 8) accordingly showed a steeper DAR decrease than did its low-DAR counterpart T-$(P_{(12\times2)}$-DM1$)_3$ (white circles in Fig. 8).

However, in the case of hydrophobic and highly aggregated ADCs, low-to-medium DAR species forming the mixtures may possess equal or similar propensity to form aggregates at stressed temperatures, thereby leveling out the effect of the more conjugated species leaving the monomer. As a result, the DAR decrease for these ADCs appears to be reduced. This hypothesis would explain why ADCs T-$(L_{24}$-DM1$)_8$ (grey diamonds in Fig. 8) and T-(MCC-DM1$)_7$ (white triangles in Fig. 8) showed a DAR loss comparable with their low-DAR counterparts T-$(L_{24}$-DM1$)_3$ (white diamonds in Fig. 8) and Kadcyla® (white squares in Fig. 8).

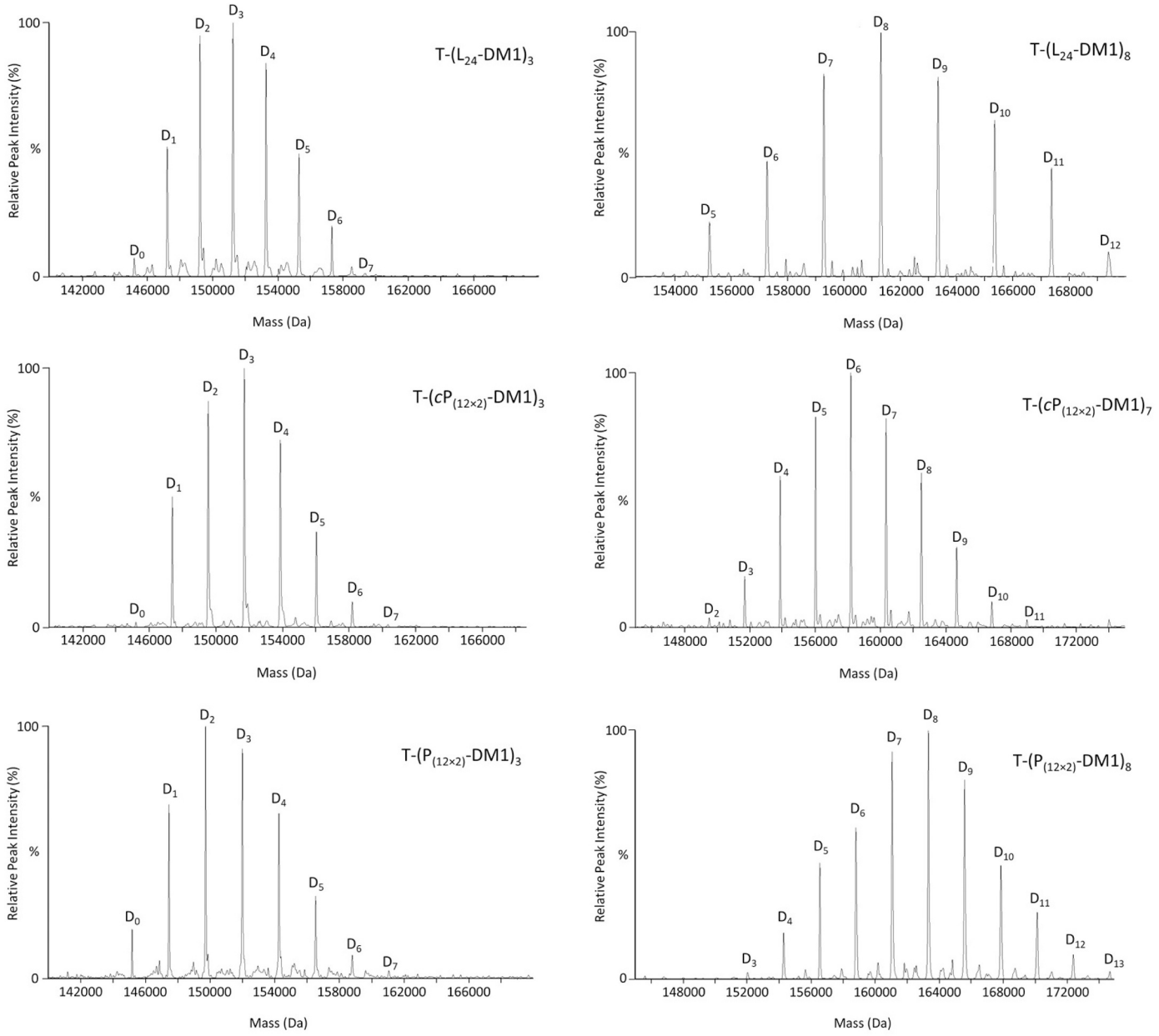

Fig. 6. Representative drug distribution profiles of the ADCs prepared *via* the one-step bioconjugation procedure.

While a linear trend was observed for all the amide-coupled ADCs (square of the correlation coefficient: r^2 = 0.97102 on average), carbamate-coupled ADCs T-($cP_{(12\times2)}$-DM1)$_3$ and T-($cP_{(12\times2)}$-DM1)$_7$ exhibited a biphasic DAR decrease kinetic (plain lines in Fig. 8). As will be discussed later, the reduction of the DAR of these two conjugates was also caused by a huge and sudden release of DM1-related species (*i.e.*, DM1-linker moiety) from the ADCs, added to the progressive and slower loss of high DAR species from the monomer.

Non-reducing SDS-PAGE gels of T-(L_{24}-DM1)$_3$, T-(L_{24}-DM1)$_8$, T-($P_{(12\times2)}$-DM1)$_3$, and T-($P_{(12\times2)}$-DM1)$_8$ revealed that most aggregates detected under the native SEC-HPLC conditions were most likely present as non-covalently associated mAb molecules as the four PEGylated ADCs migrated predominantly as a single band of approximately 150 kDa, corresponding to the full antibody molecule (lanes 3, 5, 6, 7 in Fig. 9a). Only faded bands of approximately 300 kDa could be detected under the denaturing, non-reducing SDS-PAGE conditions of the 28-day thermally stressed samples (Fig. 9a). In addition to the band corresponding to the intact mAb, Kadcyla® presented a clear band of approximately 300 kDa (lane 2 in Fig. 9a), which indicated that the aggregates in Kadcyla® were, at least partially, linked *via* covalent bonds. Under reducing conditions, predominantly a single HC band migrating at approximately 50 kDa and an LC band migrating at approximately 25 kDa were observed in all the samples (Fig. 9b). In the PEGylated ADCs, the conjugated light chains migrated as a resolved band, hydrodynamically larger than the unconjugated LC band. Minor bands migrating approximately at ~85, 120, and 140 kDa were observed on all the stressed samples (Trs included) but were much more intense and clearer in Kadcyla® (Fig. 9b, lane 2). The appearance of these minor species in reducing conditions is consistent with HC and LC fragments whose disulfide bonds have been reduced by the reducing treatment and are now kept together by covalent, non-reducible bonds. Interchain cross-links mediated by the maleimide heads of residual unreacted linkers in Kadcyla® can contribute to the formation of these aggregates, as it has been proposed for SMCC-modified Trs conjugates [41,46]. Lacking unconjugated linker species (see mass analysis), other mechanisms – either intermolecular or intramolecular – have to come into play in the case of our ADCs.

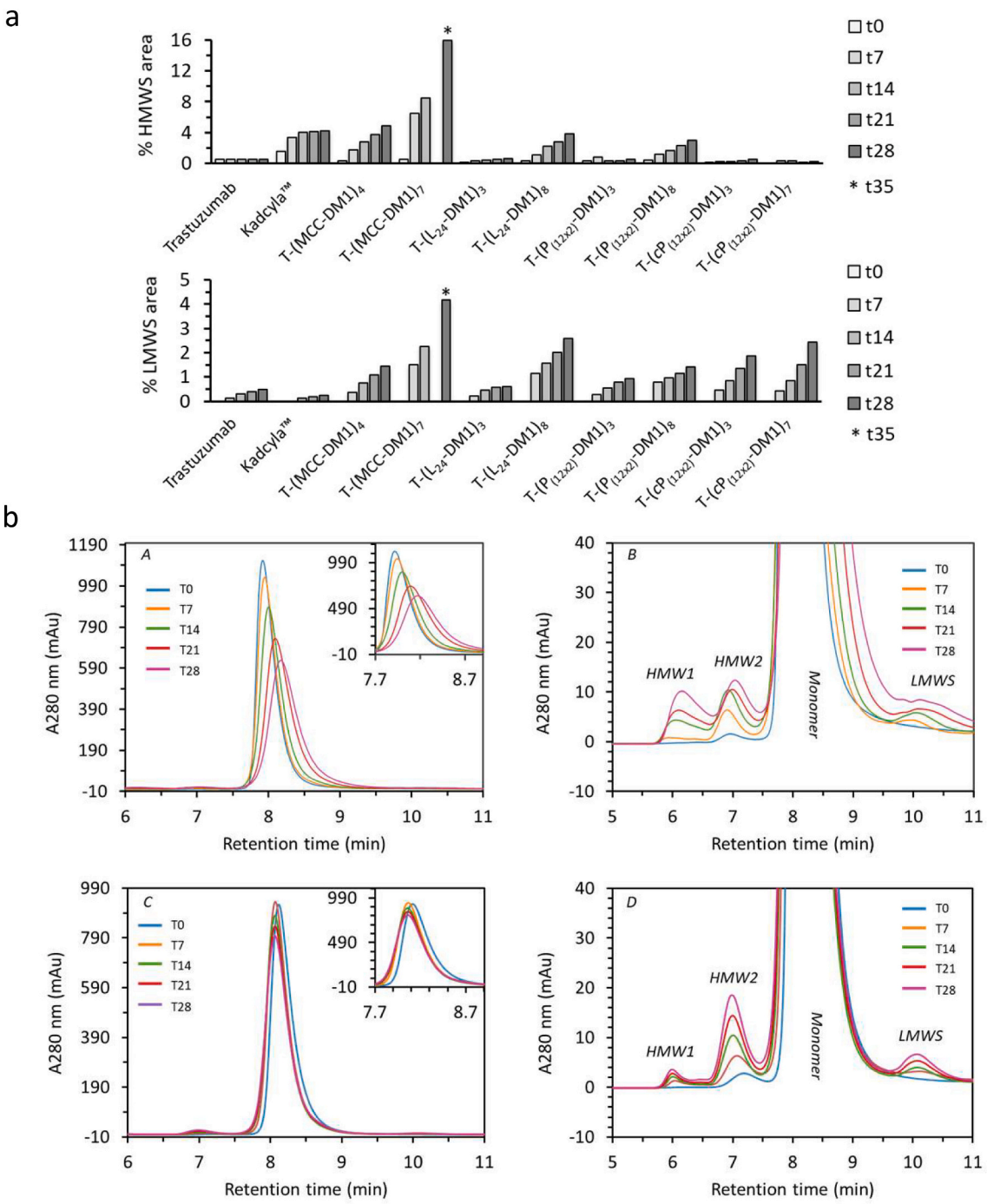

Fig. 7. a) HMWS areas (upper panel) and LMWS areas (lower panel) as a percentage of the initial total area over 4 weeks at 40 °C. b) SEC chromatograms (λ = 280 nm) either representing the change of the monomer or focusing on HMWS and LMWS at every time point for T-$(L_{24}$-DM1$)_8$ (A and B) and T-$(P_{(12\times2)}$-DM1$)_8$ (C and D).

The amount of free DM1 and/or DM1-related species in the thermally stressed ADCs was determined by RP-HPLC analysis following protein precipitation with ice-cold acetone. The species were quantified using a standard curve generated with serial dilutions of DM1 standard stock solution. In the case of the amide-coupled ADCs T-$(L_{24}$-DM1$)_3$, T-$(L_{24}$-DM1$)_9$, T-$(P_{(12\times2)}$-DM1$)_3$, T-$(P_{(12\times2)}$-DM1$)_8$, T-(MCC-DM1$)_3$, T-(MCC-DM1$)_7$ and Kadcyla®, the impurity was in the form of two peaks of DM1-linker-COOH isomers (note that ADC T-$(L_{24}$-DM1$)_9$ was part of a different battery of conjugates tested on a preliminary 28-day experiment). As shown in Fig. 10, a time-dependent increase of the said species was observed in all the samples, which indicated that a progressive shedding from the antibody – *via* hydrolysis of the DM1-linker covalently linked to the antibody and/or loss of the DM1-linker-COOH non-covalently associated with the antibody – occurred during the stability study. However, the content of such impurity at the end of the study was only ≤6% of the total DM1 (Fig. 10), in line with usual levels of unconjugated drug-related species found in ADCs manufactured by lysine amide coupling [47]. In the case of the two carbamate-coupled ADCs T-$(cP_{(12\times2)}$-DM1$)_3$ and T-$(cP_{(12\times2)}$-DM1$)_7$, the impurity was in the form of DM1-MAP12-OH, plausibly after decarboxylation of the species DM1-MAP12-OC(=O)OH, plus two other peaks which could be identified as DM1-containing species by three characteristic in-source fragmentation ion (*m/z* 435.18, 485.22, and 547.22) that are observed in all DM1 containing mass spectra. As shown in Fig. 10, the said species

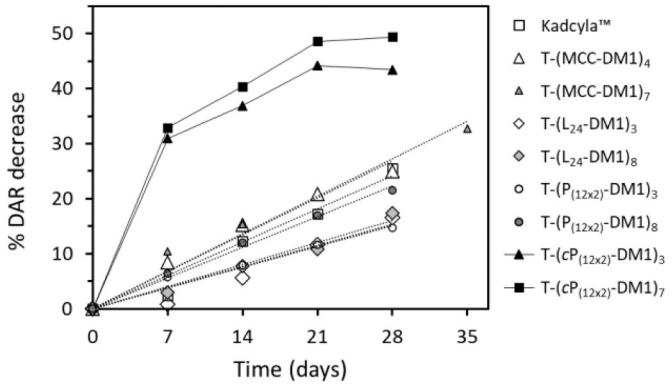

Fig. 8. Percent DAR decrements over the 28-day experiment for amide-coupled and carbamate-coupled ADCs. Dotted lines highlight linear trends. Plain lines highlight non-linear trends.

appeared to follow a biphasic release, with a rapid growth within the first week followed by a shallower increase at later time points (t7-t28) and accounted for >20% of the total DM1 at the end of the study (Fig. 10). In face of such a critical chemical instability, we postulated that the drug-linker DM1-MAP12NP had bound, to an unusual extent (about 0.9 and 2.0 mol per mole of antibody in T-($cP_{(12\times2)}$-DM1)$_3$ and T-($cP_{(12\times2)}$-DM1)$_7$, respectively) to an amino acid other than lysine on Trs, likely histidine [48,49], resulting in the formation of a labile and hydrolysable linkage that caused the detachment of a fraction of DM1-linker from the antibody. Investigating the stability of this linker, we observed that the conjugate formed with benzylamine remains stable under the pH range tested in the solution stability study (pH 5), which suggests that the MAP12NP linker forms stable bonds with primary amines (data not shown). Consequently, the instability observed in the solution stability study has to be related to the conjugation with a different amino group. Although the identification of the amino acid residue involved in this labile bond was not addressed by our team, we considered this level of unconjugated drug unacceptable and discontinued the work on ADCs based on the MAP12NP linker.

3.1.2. Pharmacokinetics

To evaluate whether the introduction of two pendant 12-unit PEG molecules in the maytansinoid-linker structure would translate to reduced systemic clearance and improved *in vivo* exposure,

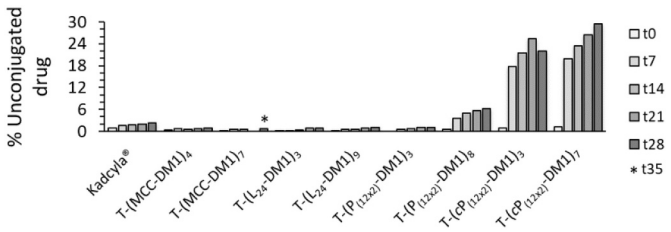

Fig. 10. Unconjugated DM1-linker species found in the ADC samples, calculated at each time point as a fractional value of the total drug of the unstressed ADC solution. Data sets of the linear PEGylated ADC T-(L_{24}-DM1)$_9$ were gathered in a preliminary 28-day experiment.

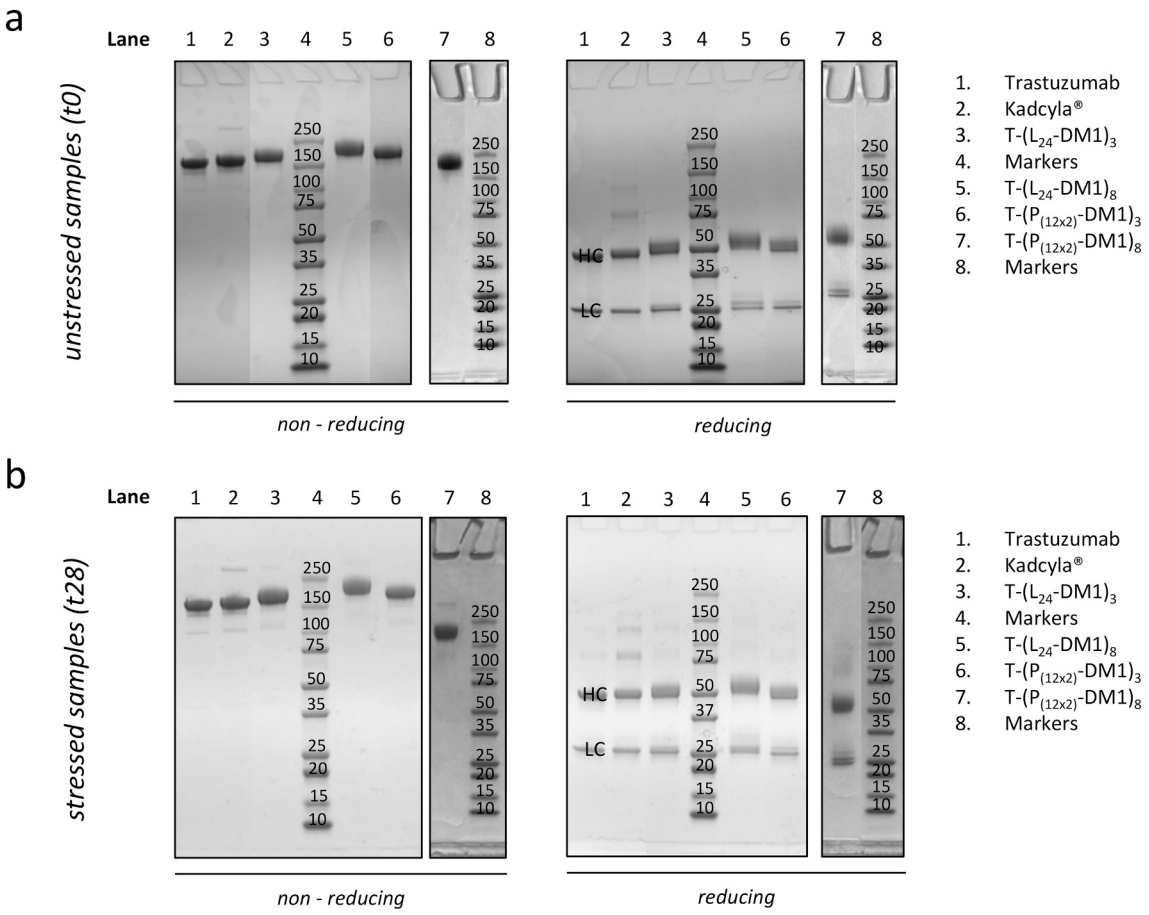

Fig. 9. Reducing and non-reducing SDS-PAGE performed using Coomassie blue stain. a) t0, unstressed samples; b) t28, 40 °C stressed samples. (Lane 1) Trs, (Lane 2) Kadcyla®, (Lane 3) T-(L_{24}-DM1)$_3$, (Lane 5) T-(L_{24}-DM1)$_8$, (Lane 6) T-($P_{(12\times2)}$-DM1)$_3$, (Lane 7) T-($P_{(12\times2)}$-DM1)$_8$. Markers are in lanes 4 and 8. (For interpretation of the references to color in this figure legend, the reader is referred to the web version of this article.)

pharmacokinetic analyses in mice were conducted with T-(L_{24}-DM1)$_3$, T-(L_{24}-DM1)$_8$, T-($P_{(12\times2)}$-DM1)$_3$ and T-($P_{(12\times2)}$-DM1)$_8$; Kadcyla® was tested as control ADC bearing no PEG molecule in the linker structure. ADCs T-(L_{24}-DM1)$_3$ and T-($P_{(12\times2)}$-DM1)$_3$ showed a similar clearance profile (Fig. 11), with a statistically significant difference in the plasmatic concentration only at the latest time point, which suggested that the impact of the PEG configuration on the ADC disposition may be negligible at usual drug loadings. The former had a slower distribution phase but a slightly steeper elimination phase than the latter, as indicated by the rate constants k_β in Table 5. This resulted in half-lives $t_{1/2}$ (β) of 9.1 d and 10.5 d for T-(L_{24}-DM1)$_3$ and T-($P_{(12\times2)}$-DM1)$_3$, respectively (Table 5). The inclusion of a PEG unit, either linear or pendant, seemed to be anyhow beneficial as both T-(L_{24}-DM1)$_3$ and T-($P_{(12\times2)}$-DM1)$_3$ had almost a 2-fold greater ADC exposure than the non-PEGylated Kadcyla® (AUC in Table 5). That being said, only T-($P_{(12\times2)}$-DM1)$_3$ had a statistically significantly higher plasmatic concentration than Kadcyla® at the latest time point.

The anticipated difference between the two PEG configurations came to light when comparing the two DAR 8 ADCs T-(L_{24}-DM1)$_8$ and T-($P_{(12\times2)}$-DM1)$_8$ (Fig. 11, Table 5). We were pleased to note that the inclusion of two 12-unit pendant PEG molecules within the linker scaffold resulted in statistically significantly higher plasmatic concentrations of the DAR 8 ADC than did the incorporation of 24-unit linear PEG molecule (Fig. 11); the linear conjugate T-(L_{24}-DM1)$_8$ was eliminated faster and had almost 3-times lower AUC than the pendant conjugate T-($P_{(12\times2)}$-DM1)$_8$ (Table 5). In comparison to its low-DAR companion, the linear conjugate T-(L_{24}-DM1)$_8$ showed a 4-fold increase in clearance (0.29 to 1.17 mL h^{-1} kg^{-1}) and a 2.8-fold increase in the volume of distribution V_β (94 to 244 mL/kg). The accelerated plasma clearance of ADC T-(L_{24}-DM1)$_8$ led to a dramatic decrease in exposure ($AUC_{0\text{-inf}}$ 356 *versus* 1446 μg mL^{-1} d^{-1}), which was also 2-fold lower than that of Kadcyla® ($AUC_{0\text{-inf}}$ 356 *versus* 737 μg mL^{-1} d^{-1}). Conversely, the high-DAR pendant conjugate T-($P_{(12\times2)}$-DM1)$_8$ showed a PK profile similar to that of its low-DAR companion, with no statistically significant difference in the plasmatic concentrations of the two during the whole PK. More specifically, the $AUC_{0\text{-inf}}$ of the high-DAR pendant conjugate T-($P_{(12\times2)}$-DM1)$_8$ was decreased by only 1.3-fold (1051 *versus* 1356 μg mL^{-1} d^{-1}), and CL was increased accordingly from 0.31 to 0.40 μg mL^{-1} d^{-1}. ADC T-(L_{24}-DM1)$_8$. Of note, notwithstanding the high drug loading, ADC T-($P_{(12\times2)}$-DM1)$_8$ also had a greater exposure than Kadcyla® (1051 *versus* 737 μg mL^{-1} d^{-1}), with a statistically significant difference in the plasmatic concentrations of the two at the latest time point (Fig. 11).

These results confirmed that two 12-unit PEG molecules in a pendant configuration, between the antibody and DM1, can shield the hydrophobic burden derived from a profuse conjugation. The linear PEG_{24} spacer exhibited a good shielding effect at usual drug loadings but failed when the total hydrophobicity increased at higher DARs, as demonstrated elsewhere [25]. The great advantage of this pendant configuration of the polymer might be rooted in the proximity of the drug DM1 to the antibody inside a hydrophilic, highly hydrated shell created by the two pendant PEG_{12} chains.

Table 5
Summary of total Trs pharmacokinetics in plasma of one-step bioconjugated T-(L_{24}-DM1)$_3$, T-(L_{24}-DM1)$_8$, T-($P_{(12\times2)}$-DM1)$_3$, T-($P_{(12\times2)}$-DM1)$_8$ and Kadcyla® in female mice.

ADC	$t_{1/2}$ β (days)	k_β (h^{-1})	V_β (mL/kg)	CL (mL/h/kg)	$AUC_{0\text{-inf}}$ (μg/ml × d)
T-(L_{24}-DM1)$_3$	9.1	3.2 ×10^{-3}	94	0.29	1446
T-($P_{(12\times2)}$-DM1)$_3$	10.5	2.8 ×10^{-3}	113	0.31	1356
T-(L_{24}-DAR)$_8$	6.5	4.5 ×10^{-3}	244	1.17	356
T-($P_{(12\times2)}$-DM1)$_8$	9.2	3.1 ×10^{-3}	134	0.40	1051
Kadcyla®	9.4	3.1 ×10^{-3}	185	0.57	737

Abbreviations: $t_{1/2}$ β, half-life (disposition phase); k_β, rate constant of disposition; V_β, volume of distribution in disposition phase; CL, clearance; $AUC_{0\text{-inf}}$, area under the curve from time 0 to infinity.

4. Discussion

One of the major downsides of the ADCs lies in the solubility issues that arise from the conjugation of small, organic, lipophilic drug molecules to an antibody. In fact, the conjugation process *per se* and, especially, of lipophilic entities to antibodies can perturb the physical stability of the antibody [50]. This can result in the formation of inactive and potentially toxic/immunogenic aggregates, which may show undesirable tropism for healthy organs (*e.g.*, liver) and fast body clearance with a consequent failed delivery of the drug to the tumor [20,25]. The aforementioned scenario is more likely to happen for ADCs with high DARs, because the hydrophobic burden the antibody is requested to carry is too heavy to be sustained [3]. Within this context, the use of hydrophilic linkers can soothe the impact of conjugation and help maintain the antibody traits of the ADC unchanged, while permitting higher drug loads as well as the conjugation of drugs less cytotoxic than the so far exploited toxins.

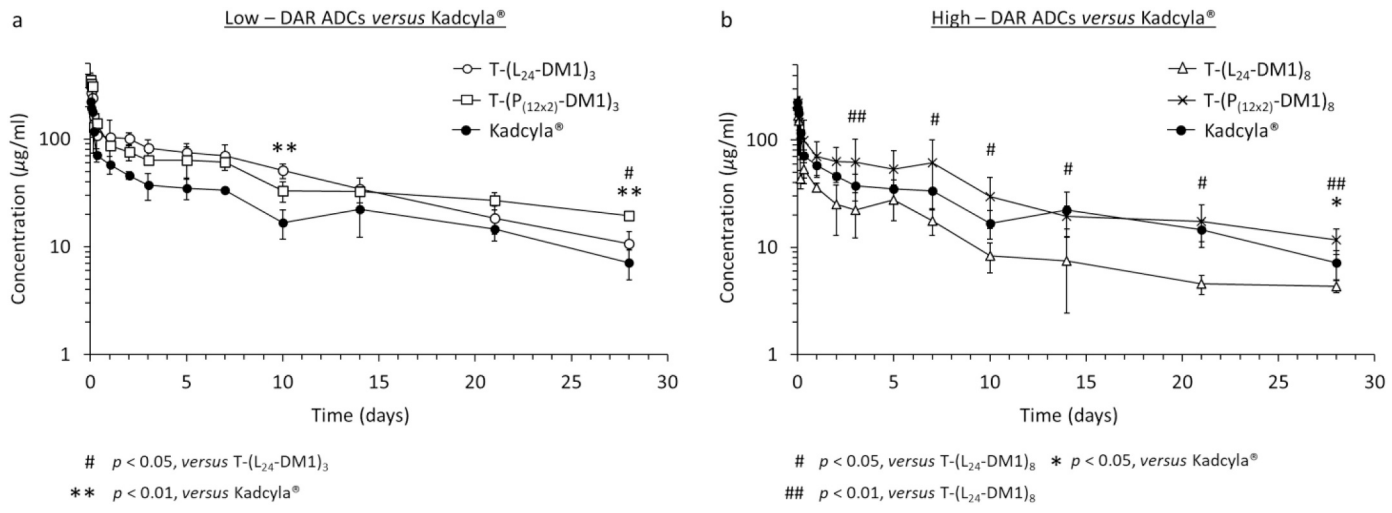

Fig. 11. a) Mean total antibody concentrations in plasma of DAR3–4 ADCs and Kadcyla® following intravenous administration at 10 mg/kg; b) Mean total antibody concentrations in plasma of DAR8 ADCs and Kadcyla® following intravenous administration at 10 mg/kg. Error bars are standard deviation.

In this study, we evaluated PEG as hydrophilicity-promoting entity, in the linkers, for the construction of highly-loaded lysine-conjugated Trs-DM1 ADCs. We focused on the effect of the configuration and positioning of the PEG unit within the linker structure on both the physical stability and the *in vivo* pharmacokinetic profile of the conjugates. To this effect, we set out to compare a conventional linear 24-unit PEG linear oligomer to two pendant 12-unit PEG chains, with the idea that the latter layout would mask the hydrophobicity of the drug more efficiently once installed onto the antibody. The SMCC linker, present in Kadcyla® (used as ADC model throughout this work), was included in this investigation as an exemplary non-PEGylated linker.

Two conjugation methods of the lysine residues on Trs were explored. When the antibody was first modified with the linker species and then reacted with the drug DM1, not all the linkers that had linked to the antibody were successfully conjugated by the drug in the ensuing conjugation reaction (Table 2). We postulated that the drug DM1 was somehow impeded from reacting with the maleimide ends of the linker-modified antibodies. In this approach, the linker-modified antibody was required to have an average number of linkers (linker-to-antibody ratio or LAR in the text) greater than the average DAR that was intended to be reached. For instance, an average of 6.1 linkers per antibody was needed to achieve an average DAR of 3.8 in the T-(MCC-DM1)$_3$ ADC. The longer PEGylated linker MAL24PS seemed to show higher reactivity likely because its maleimide head, protruding further out the antibody microenvironment, was more available to the thiol-containing DM1. Mass analysis of the conjugates obtained with this approach allowed us to easily identify these unconjugated linker-modified antibody species and estimate their abundance relative to the total linker content in each conjugate (Fig. 3, Eqs. 4–6).

In the second conjugation method, the linker/DM1 coupling was conducted before the conjugation of the antibody amines. We exploited the rapid (1 h) and quantitative formation of PEGylated linkers-DM1 intermediates, with high yields (> 70%), and directly use the reaction mixtures for the conjugation with Trs (Table 3, Figs. 4–5). The conversion rate of the linker to the linker-DM1 was key to achieve the desired DAR values in the subsequent conjugation step with the antibody. In the case of non-PEG linkers, to overcome the solubility issues of the DM1-SMCC in the reaction mixture with the antibody we isolated the intermediate by flash silica chromatography. The use of pre-conjugated DM1-SMCC – combined with slow addition to the antibody solution while stirring – solved the precipitation problem upon addition to Trs solution – we estimated that a good range of solubility of DM1-SMCC in 10% (*v*/v) DMA/borate buffer is approximately 0.7–0.9 mg/mL.

The ADCs obtained *via* this second approach did not exhibit subpopulations with unconjugated linkers appended on the antibody, which confirmed that this synthetic route is a better alternative to the 2-step conjugation method of Kadcyla® in achieving less heterogeneous ADC mixtures (Fig. 6). In the case of the PEG-containing ADCs, we used discrete PEGs with precise control of the number of ethylene glycol units (*i.e.*, PEG molecular weight) for optimal preparation of structurally defined conjugates.

Evaluation of the ADCs for their physical stability and chemical integrity in solution revealed that the presence and configuration of the PEG unit (linear or pendant) and the type of Trs-linker bonding (amide or carbamate) are of great importance for stability. The SMCC linker (*i.e.*, without PEG) could not generate stable ADCs with DARs above 4 (Fig. 7a), owing to a marked tendency to aggregation. ADCs prepared with the pendant-PEG linker MAP12PS demonstrated higher stability under the conditions (stress temperature of 40 °C) than ADCs with the linear-PEG linker MAL24PS (Figs. 7a–7b). When the DAR was increased from 3 to 8, the ADC monomer content after 28 days was reduced by 11% in T-(L_{24}-DM1)$_8$ and only by 4% in T-($P_{(12\times2)}$-DM1)$_8$. The aggregate composition of the two stressed ADC after 28-days was different, with a greater abundance of bigger aggregates in the linear conjugate T-(L_{24}-DM1)$_8$ (*i.e.*, HMW1 in chromatograms B and D in Fig. 7b). We also observed a milder variation of the DAR of the monomer throughout the study (Fig. 8) for T-(L_{24}-DM1)$_8$, suggesting that the ADC isomers with different DARs have a similar tendency to aggregate. Conversely, in the case of T-($P_{(12\times2)}$-DM1)$_8$ the high DAR species showed a higher tendency to aggregate, thereby resulting in a more evident DAR decrease of the monomer (Fig. 8). Measurement of average DAR variation during SEC analysis (Fig. 8) and free drug analysis (Fig. 10) disclosed a pronounced chemical instability of the carbamate-coupled ADCs T-($cP_{(12\times2)}$-DM1)$_3$ and T-($cP_{(12\times2)}$-DM1)$_7$. In both data sets, a biphasic non-linear variation was observed. We postulated that the drug-linker DM1-MAP12NP had bound to two different amino acid residues on the antibody resulting in the formation of two linkages with different stability.

In vivo pharmacokinetic profiles of the ADCs paralleled the trends in aggregation tendency observed in the stability study. ADCs featuring either the linker MAL24PS or the linker MAP12PS showed only minimal differences at DARs of about 4, confirming that there may be similar benefits from using linear or pendant configurations in the construction of low-DAR ADCs (Fig. 11 and Table 5). Significant differences in the plasma clearance were instead observed at higher DARs (about 8). The 24-unit PEG molecule in a linear layout was unable to shield this high hydrophobic burden, thereby revealing the limitation of using such configuration when aiming at high DARs. By contrast, the two 12-unit PEG molecules in a pendant and orthogonal orientation to the drug proved to be a consistent hydrophilicity-promoting entity, capable of efficiently maintaining the PK properties. As previously stated in the text, the great advantage of this arrangement may be rooted in the proximity of DM1 to the antibody covered by a hydrated shell created by the two pendant PEG_{12} chains.

5. Conclusions

We have explored the potential of using PEG-based linkers for the preparation of hydrophilic highly loaded lysine-conjugated ADCs. This study demonstrates that the configuration of PEG in the linkers of ADCs influences the *in vivo* pharmacokinetic and stability in solution of lysine-conjugated ADCs. We were able to prove that a linker containing two pendant 12-unit PEG chains can represent an optimal hydrophilic reservoir for the construction of high drug-loaded ADCs with decreased aggregation tendency and favorable pharmacokinetic characteristics. Owing to its simplicity, lysine-based conjugation, with a first linker drug conjugation step followed by the antibody conjugation step, has proven to be a valid and useful conjugation strategy within the linker selection process. Motivated by these findings, we are currently focusing on the evaluation and development of peptide-cleavable variants of this novel pendant PEG technology.

Authors contributions

TT: design of the experiments, collection and assembling of the data, data analysis and interpretation, manuscript writing. BC: collection and assembling of the data, data analysis. AG: data analysis. MB: Mass spectrometry analysis and interpretation. MS: contribution in animal experiments. YM, AS, HY: synthesis of linker, data analysis and interpretation. GP: conception and design, data assembling, analysis and interpretation, manuscript writing.

Acknowledgements

The research was supported by NOF Corporation. GP's Lab is also supported from AIRC under IG 2017 - ID. 20244 project – P.I. Pasut Gianfranco.

Appendix A. Supplementary data

Supplementary data to this article can be found online at https://doi.org/10.1016/j.jconrel.2021.07.041.

References

[1] R.V.J. Chari, M.L. Miller, W.C. Widdison, Antibody-drug conjugates: an emerging concept in cancer therapy, Angew. Chemie - Int. Ed. 53 (2014) 3796–3827, https://doi.org/10.1002/anie.201307628.

[2] A. Beck, L. Goetsch, C. Dumontet, N. Corvaïa, Strategies and challenges for the next generation of antibody-drug conjugates, Nat. Rev. Drug Discov. 16 (2017) 315–337, https://doi.org/10.1038/nrd.2016.268.

[3] P.M. Drake, D. Rabuka, Recent developments in ADC technology: preclinical studies signal future clinical trends, BioDrugs. 31 (2017) 521–531, https://doi.org/10.1007/s40259-017-0254-1.

[4] P.D. Senter, E.L. Sievers, The discovery and development of brentuximab vedotin for use in relapsed Hodgkin lymphoma and systemic anaplastic large cell lymphoma, Nat. Biotechnol. 30 (2012) 631–637, https://doi.org/10.1038/nbt.2289.

[5] J.M. Lambert, R.V.J. Chari, Ado-trastuzumab Emtansine (T-DM1): an antibody-drug conjugate (ADC) for HER2-positive breast cancer, J. Med. Chem. 57 (2014) 6949–6964, https://doi.org/10.1021/jm500766w.

[6] C.H. Chau, P.S. Steeg, W.D. Figg, Antibody–drug conjugates for cancer, Lancet. 394 (2019) 793–804, https://doi.org/10.1016/S0140-6736(19)31774-X.

[7] E.D. Deeks, Polatuzumab vedotin: first global approval, Drugs. 79 (2019) 1467–1475, https://doi.org/10.1007/s40265-019-01175-0.

[8] S.J. Keam, Trastuzumab deruxtecan: first approval, Drugs. 80 (2020) 501–508, https://doi.org/10.1007/s40265-020-01281-4.

[9] A. Markham, Belantamab mafodotin: first approval, Drugs. 80 (2020) 1607–1613, https://doi.org/10.1007/s40265-020-01404-x.

[10] Y.Y. Syed, Sacituzumab govitecan: first approval, Drugs. 80 (2020) 1019–1025, https://doi.org/10.1007/s40265-020-01337-5.

[11] E. Chang, C. Weinstock, L. Zhang, R. Charlab, S.E. Dorff, Y. Gong, V. Hsu, F. Li, T. K. Ricks, P. Song, S. Tang, P.E. Waldron, J. Yu, E. Zahalka, K.B. Goldberg, R. Pazdur, M.R. Theoret, A. Ibrahim, J.A. Beaver, FDA approval summary: enfortumab vedotin for locally advanced or metastatic urothelial carcinoma, Clin. Cancer Res. 27 (2021) 922–927, https://doi.org/10.1158/1078-0432.CCR-20-2275.

[12] M. Damelin, W. Zhong, J. Myers, P. Sapra, Evolving strategies for target selection for antibody-drug conjugates, Pharm. Res. 32 (2015) 3494–3507, https://doi.org/10.1007/s11095-015-1624-3.

[13] S.C. Alley, D.R. Benjamin, S.C. Jeffrey, N.M. Okeley, D.L. Meyer, R.J. Sanderson, P. D. Senter, Contribution of linker stability to the activities of anticancer immunoconjugates, Bioconjug. Chem. 19 (2008) 759–765, https://doi.org/10.1021/bc7004329.

[14] B.A. Kellogg, L. Garrett, Y. Kovtun, K.C. Lai, B. Leece, M. Miller, G. Payne, R. Steeves, K.R. Whiteman, W. Widdison, H. Xie, R. Singh, R.V.J. Chari, J. M. Lambert, R.J. Lutz, Disulfide-linked antibody-maytansinoid conjugates: optimization of in vivo activity by varying the steric hindrance at carbon atoms adjacent to the disulfide linkage, Bioconjug. Chem. 22 (2011) 717–727, https://doi.org/10.1021/bc100480a.

[15] G. Badescu, P. Bryant, M. Bird, K. Henseleit, J. Swierkosz, V. Parekh, R. Tommasi, E. Pawlisz, K. Jurlewicz, M. Farys, N. Camper, X. Sheng, M. Fisher, R. Grygorash, A. Kyle, A. Abhilash, M. Frigerio, J. Edwards, A. Godwin, Bridging disulfides for stable and defined antibody drug conjugates, Bioconjug. Chem. 25 (2014) 1124–1136.

[16] R.P. Lyon, J.R. Setter, T.D. Bovee, S.O. Doronina, J.H. Hunter, M.E. Anderson, C. L. Balasubramanian, S.M. Duniho, C.I. Leiske, F. Li, P.D. Senter, Self-hydrolyzing maleimides improve the stability and pharmacological properties of antibody-drug conjugates, Nat. Biotechnol. 32 (2014) 1059–1062, https://doi.org/10.1038/nbt.2968.

[17] P.M. Drake, D. Rabuka, An emerging playbook for antibody-drug conjugates: lessons from the laboratory and clinic suggest a strategy for improving efficacy and safety, Curr. Opin. Chem. Biol. 28 (2015) 174–180, https://doi.org/10.1016/j.cbpa.2015.08.005.

[18] B.Q. Shen, K. Xu, L. Liu, H. Raab, S. Bhakta, M. Kenrick, K.L. Parsons-Reponte, J. Tien, S.F. Yu, E. Mai, D. Li, J. Tibbitts, J. Baudys, O.M. Saad, S.J. Scales, P. J. McDonald, P.E. Hass, C. Eigenbrot, T. Nguyen, W.A. Solis, R.N. Fuji, K. M. Flagella, D. Patel, S.D. Spencer, L.A. Khawli, A. Ebens, W.L. Wong, R. Vandlen, S. Kaur, M.X. Sliwkowski, R.H. Scheller, P. Polakis, J.R. Junutula, Conjugation site modulates the in vivo stability and therapeutic activity of antibody-drug conjugates, Nat. Biotechnol. 30 (2012) 184–189, https://doi.org/10.1038/nbt.2108.

[19] K.J. Hamblett, P.D. Senter, D.F. Chace, M.M.C. Sun, J. Lenox, C.G. Cerveny, K. M. Kissler, S.X. Bernhardt, A.K. Kopcha, R.F. Zabinski, D.L. Meyer, J.A. Francisco, Effects of drug loading on the antitumor activity of a monoclonal antibody drug conjugate, Clin. Cancer Res. 10 (2004) 7063–7070, https://doi.org/10.1158/1078-0432.CCR-04-0789.

[20] X. Sun, J.F. Ponte, N.C. Yoder, R. Laleau, J. Coccia, L. Lanieri, Q. Qiu, R. Wu, E. Hong, M. Bogalhas, L. Wang, L. Dong, Y. Setiady, E.K. Maloney, O. Ab, X. Zhang, J. Pinkas, T.A. Keating, R. Chari, H.K. Erickson, J.M. Lambert, Effects of drug-antibody ratio on pharmacokinetics, biodistribution, efficacy, and tolerability of antibody-maytansinoid conjugates, Bioconjug. Chem. 28 (2017) 1371–1381, https://doi.org/10.1021/acs.bioconjchem.7b00062.

[21] A.A. Wakankar, M.B. Feeney, J. Rivera, Y. Chen, M. Kim, V.K. Sharma, Y.J. Wang, Physicochemical stability of the antibody - drug conjugate trastuzumab-DM1: changes due to modification and conjugation processes, Bioconjug. Chem. 21 (2010) 1588–1595, https://doi.org/10.1021/bc900434c.

[22] N.S. Beckley, K.P. Lazzareschi, H.W. Chih, V.K. Sharma, H.L. Flores, Investigation into temperature-induced aggregation of an antibody drug conjugate, Bioconjug. Chem. 24 (2013) 1674–1683, https://doi.org/10.1021/bc400182x.

[23] A.V. Gandhi, K.J. Arlotta, H.N. Chen, S.C. Owen, J.F. Carpenter, Biophysical properties and heating-induced aggregation of lysine-conjugated antibody-drug conjugates, J. Pharm. Sci. 107 (2018) 1858–1869, https://doi.org/10.1016/j.xphs.2018.03.022.

[24] S.O. Doronina, J.R. Setter, T.D. Bovee, M.E. Anderson, M. Jonas, S. Daniho, H. Kostner, P.D. Senter, R.P. Lyon, Abstract 4470: elucidating the role of drug-linker hydrophobicity in the disposition of antibody-drug conjugates, Cancer Res. 74 (2014) 4470, https://doi.org/10.1158/1538-7445.AM2014-4470.

[25] R.P. Lyon, T.D. Bovee, S.O. Doronina, P.J. Burke, J.H. Hunter, H.D. Neff-Laford, M. Jonas, M.E. Anderson, J.R. Setter, P.D. Senter, Reducing hydrophobicity of homogeneous antibody-drug conjugates improves pharmacokinetics and therapeutic index, Nat. Biotechnol. 33 (2015) 733–735, https://doi.org/10.1038/nbt.3212.

[26] R.Y. Zhao, S.D. Wilhelm, C. Audette, G. Jones, B.A. Leece, A.C. Lazar, V. S. Goldmacher, R. Singh, Y. Kovtun, W.C. Widdison, J.M. Lambert, R.V.J. Chari, Synthesis and evaluation of hydrophilic linkers for antibody-maytansinoid conjugates, J. Med. Chem. 54 (2011) 3606–3623, https://doi.org/10.1021/jm2002958.

[27] N. Bodyak, A.V. Yurkovetskiy, Delivering more oayload (high DAR ADCs), in: Cancer Drug Discov. Dev, Humana Press, Cham, 2018, pp. 215–240, https://doi.org/10.1007/978-3-319-78154-9_9.

[28] Y. Ogitani, K. Hagihara, M. Oitate, H. Naito, T. Agatsuma, Bystander killing effect of DS-8201a, a novel anti-human epidermal growth factor receptor 2 antibody–drug conjugate, in tumors with human epidermal growth factor receptor 2 heterogeneity, Cancer Sci. 107 (2016) 1039–1046, https://doi.org/10.1111/cas.12966.

[29] P.J. Burke, J.Z. Hamilton, S.C. Jeffrey, J.H. Hunter, S.O. Doronina, N.M. Okeley, J. B. Miyamoto, M.E. Anderson, I.J. Stone, M.L. Ulrich, J.K. Simmons, E.E. McKinney, P.D. Senter, R.P. Lyon, Optimization of a PEGylated glucuronide-monomethylauristatin E linker for antibody–drug conjugates, Mol. Cancer Ther. 16 (2017) 116–123, https://doi.org/10.1158/1535-7163.MCT-16-0343.

[30] M. Pabst, W. McDowell, A. Manin, A. Kyle, N. Camper, E. De Juan, V. Parekh, F. Rudge, H. Makwana, T. Kantner, H. Parekh, A. Michelet, X.B. Sheng, G. Popa, C. Tucker, F. Khayrzad, D. Pollard, K. Kozakowska, R. Resende, A. Jenkins, F. Simoes, D. Morris, P. Williams, G. Badescu, M.P. Baker, M. Bird, M. Frigerio, A. Godwin, Modulation of drug-linker design to enhance in vivo potency of homogeneous antibody-drug conjugates, J. Control. Release 253 (2017) 160–164, https://doi.org/10.1016/j.jconrel.2017.02.027.

[31] S.V. Govindan, T.M. Cardillo, E.A. Rossi, P. Trisal, W.J. McBride, R.M. Sharkey, D. M. Goldenberg, Improving the therapeutic index in cancer therapy by using antibody-drug conjugates designed with a moderately cytotoxic drug, Mol. Pharm. 12 (2015) 1836–1847, https://doi.org/10.1021/mp5006195.

[32] Y.V. Kovtun, C.A. Audette, M.F. Mayo, G.E. Jones, H. Doherty, E.K. Maloney, H. K. Erickson, X. Sun, S. Wilhelm, O. Ab, K.C. Lai, W.C. Widdison, B. Kellogg, H. Johnson, J. Pinkas, R.J. Lutz, R. Singh, V.S. Goldmacher, R.V.J. Chari, Antibody-maytansinoid conjugates designed to bypass multidrug resistance, Cancer Res. 70 (2010) 2528–2537, https://doi.org/10.1158/0008-5472.CAN-09-3546.

[33] P. Strop, K. Delaria, D. Foletti, J.M. Witt, A. Hasa-Moreno, K. Poulsen, M.G. Casas, M. Dorywalska, S. Farias, A. Pios, V. Lui, R. Dushin, D. Zhou, T. Navaratnam, T. T. Tran, J. Sutton, K.C. Lindquist, B. Han, S.H. Liu, D.L. Shelton, J. Pons, A. Rajpal, Site-specific conjugation improves therapeutic index of antibody drug conjugates with high drug loading, Nat. Biotechnol. 33 (2015) 694–696, https://doi.org/10.1038/nbt.3274.

[34] M.R. Levengood, X. Zhang, J.H. Hunter, K.K. Emmerton, J.B. Miyamoto, T.S. Lewis, P.D. Senter, Orthogonal cysteine protection enables homogeneous multi-drug antibody–drug conjugates, Angew. Chemie - Int. Ed. 56 (2017) 733–737, https://doi.org/10.1002/anie.201608292.

[35] A.V. Yurkovetskiy, M. Yin, N. Bodyak, C.A. Stevenson, J.D. Thomas, C. E. Hammond, L.L. Qin, B. Zhu, D.R. Gumerov, E. Ter-Ovanesyan, A. Uttard, T. B. Lowinger, A polymer-based antibody-vinca drug conjugate platform: characterization and preclinical efficacy, Cancer Res. 75 (2015) 3365–3372, https://doi.org/10.1158/0008-5472.CAN-15-0129.

[36] G. Pasut, F.M. Veronese, State of the art in PEGylation: the great versatility achieved after forty years of research, J. Control. Release 161 (2012) 461–472, https://doi.org/10.1016/j.jconrel.2011.10.037.

[37] S. Zalipsky, G. Pasut, Evolution of polymer conjugation to proteins, in: S. Zalipsky, G. Pasut (Eds.), Polym. Conjug, Elsevier, 2020, pp. 3–22, https://doi.org/10.1016/b978-0-444-64081-9.00001-2.

[38] P.L. Turecek, J. Siekmann, PEG–protein conjugates, in: G. Pasut, S. Zalipsky (Eds.), Polym. Conjug, 1st ed, Elsevier, 2020, pp. 61–101, https://doi.org/10.1016/B978-0-444-64081-9.00004-8.

[39] W. Viricel, G. Fournet, S. Beaumel, E. Perrial, S. Papot, C. Dumontet, B. Joseph, Monodisperse polysarcosine-based highly-loaded antibody-drug conjugates, Chem. Sci. 10 (2019) 4048–4053, https://doi.org/10.1039/C9SC00285E.

[40] W.C. Widdison, J.F. Ponte, J.A. Coccia, L. Lanieri, Y. Setiady, L. Dong, A. Skaletskaya, E.E. Hong, R. Wu, Q. Qiu, R. Singh, P. Salomon, N. Fishkin, L. Harris, E.K. Maloney, Y. Kovtun, K. Veale, S.D. Wilhelm, C.A. Audette, J. A. Costoplus, R.V.J. Chari, Development of anilino-maytansinoid ADCs that efficiently release cytotoxic metabolites in cancer cells and induce high levels of bystander killing, Bioconjug. Chem. 26 (2015) 2261–2278, https://doi.org/10.1021/acs.bioconjchem.5b00430.

[41] Y. Chen, M.T. Kim, L. Zheng, G. Deperalta, F. Jacobson, Structural characterization of cross-linked species in trastuzumab emtansine (Kadcyla), Bioconjug. Chem. 27 (2016) 2037–2047, https://doi.org/10.1021/acs.bioconjchem.6b00316.
[42] Y. Zhang, M. Huo, J. Zhou, S. Xie, PKSolver: an add-in program for pharmacokinetic and pharmacodynamic data analysis in Microsoft excel, Comput. Methods Prog. Biomed. 99 (2010) 306–314, https://doi.org/10.1016/j.cmpb.2010.01.007.
[43] J.M. Lambert, R.V.J. Chari, Ado-trastuzumab emtansine (T-DM1): an antibody – drug conjugate (ADC) for HER2-positive breast cancer, J. Med. Chem. 57 (2014) 6949–6964.
[44] M.T. Kim, Y. Chen, J. Marhoul, F. Jacobson, Statistical modeling of the drug load distribution on trastuzumab emtansine (Kadcyla), a lysine-linked antibody drug conjugate, Bioconjug. Chem. 25 (2014) 1223–1232, https://doi.org/10.1021/bc5000109.
[45] L. Chen, L. Wang, H. Shion, C. Yu, Y.Q. Yu, L. Zhu, M. Li, W. Chen, K. Gao, In-depth structural characterization of Kadcyla® (ado-trastuzumab emtansine) and its biosimilar candidate, MAbs. 8 (2016) 1210–1223, https://doi.org/10.1080/19420862.2016.1204502.
[46] A.A. Wakankar, M.B. Feeney, J. Rivera, Y. Chen, M. Kim, V.K. Sharma, Y.J. Wang, Physicochemical stability of the antibody−drug conjugate trastuzumab-DM1: changes due to modification and conjugation processes, Bioconjug. Chem. 21 (2010) 1588–1595, https://doi.org/10.1021/bc900434c.
[47] C. Hung-Wei, G. Benson, Y. Yi, Z. Boyan, Identification of amino acid residues responsible for the release of free drug from an antibody–drug conjugate utilizing lysine–succinimidyl ester chemistry, J. Pharm. Sci. 100 (2011) 2518–2525, https://doi.org/10.1002/jps.
[48] D.C. Wylie, M. Voloch, S. Lee, Y.H. Liu, S. Cannon-Carlson, C. Cutler, B. Pramanik, Carboxyalkylated histidine is a pH-dependent product of pegylation with SC-PEG, Pharm. Res. 18 (2001) 1354–1360, https://doi.org/10.1023/A:1013006515587.
[49] G. Pasut, A. Mero, F. Caboi, S. Scaramuzza, L. Sollai, F.M. Veronese, A new PEG-β-alanine active derivative for releasable protein conjugation, Bioconjug. Chem. 19 (2008) 2427–2431, https://doi.org/10.1021/bc800281s.
[50] J.W. Buecheler, M. Winzer, J. Tonillo, C. Weber, H. Gieseler, Impact of payload hydrophobicity on the stability of antibody-drug conjugates, Mol. Pharm. 15 (2018) 2656–2664, https://doi.org/10.1021/acs.molpharmaceut.8b00177.
[51] A. Grigoletto, T. Tedeschini, E. Canato, G. Pasut, The evolution of polymer conjugation and drug targeting for the delivery of proteins and bioactive molecules, Wiley Interdiscip Rev Nanomed Nanobiotechnol. 13 (2021), e1689, https://doi.org/10.1002/wnan.1689.